

Научном већу Института за физику у Београду

Београд, 08. 10. 2018.

**Предмет: Молба за покретање поступка за избор у звање истраживач приправник**

Молим Научно веће Института за физику у Београду да у складу са Правилником о поступку и начину вредновања и квантитативном исказивању научно-истраживачких резултата истраживача покрене поступак за мој избор у звање истраживач приправник.

У прилогу достављам:

1. Мишљење руководиоца пројекта са предлогом чланова комисије за избор у звање
2. Стручну биографију
3. Преглед научне активности
4. Списак публикација
5. Уверење о уписаним докторским студијама
6. Уверења о завршеним основним и мастер студијама
7. Уверење о положеним испитима на основним и мастер студијама
8. Списак положених испита на докторским студијама и фотокопија индекса
9. Копије публикација

С поштовањем,

Андрејана Шолајић

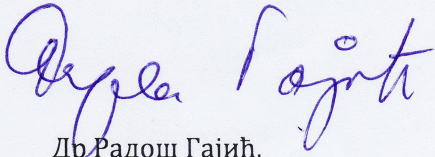
**Научном већу Института за физику у Београду**

**Предмет: Мишљење руководиоца пројекта о избору Андријане Шолајић у звање истраживач приправник**

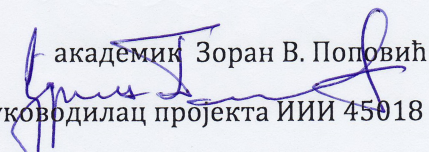
Андријана Шолајић је студент докторских студија физике, а тезу ради под менторством др Јелене Пешић. Биће ангажована на пројекту ИО171005 ("Физика уређених наноструктура и нових материјала у фотоници") са 8 истраживач месеци, и на пројекту ИИИ45018 ("Наноструктурни мултифункционални материјали и нанокомпозити") са 4 истраживач месеца, у Центру за физику чврстог стања и нове материјале, Института за физику у Београду. Докторска теза кандидаткиње биће везана за истраживање особина нових и слојевитих 2Д материјала са фокусом на њихове електронске особине и динамику решетке. С обзиром да испуњава све предвиђене услове у складу са Правилником о поступку, начину вредновања и квантитативном исказивању научноистраживачких резултата истраживача Министарства просвете, науке и технолошког развоја, сагласни смо са покретањем поступка за избор Андријане Шолајић у звање истраживач приправник.

За састав комисије за избор у звање Андријане Шолајић у звање истраживач приправник предлажемо:

- (1) др Борислав Васић, научни сарадник Института за физику у Београду
- (2) академик Зоран В. Поповић, научни саветник Института за физику у Београду,
- (3) др Радош Гајић, научни саветник Института за физику у Београду,
- (4) др Милан Тадић, редовни професор Електротехничког факултета Универзитета у Београду

  
Др Радош Гајић,

руководилац пројекта ИО 171005

  
академик Зоран В. Поповић  
руководилац пројекта ИИИ 45018

## **Стручна биографија Андријане Шолајић**

Андријана Шолајић је рођена 1991. године у Београду, где је завршила Математичку гимназију 2010. године. Дипломирала је на одсеку за Физичку електронику на Електротехничком факултету Универзитета у Београду, на смеру Наноелектроника, оптоелектроника и ласерска техника, са просеком 8.26. Дипломски рад под називом „*Електронска структура напрегнутих графенских нанотачака*“ одбранила је са оценом 10 у јуну 2016. године.

Исте године уписује мастер студије на Електротехничком факултету Универзитета у Београду, на модулу Наноелектроника и фотоника. У септембру 2017. године одбранила је мастер тезу под називом „*Одређивање електронских и фононских својстава графена допираног стронцијумом и итербијумом ДФТ методом*“, чиме завршава мастер студије са просечном оценом 10.0. Мастер рад је комплетно урађен у Центру за физику чврстог стања и нове материјале, Института за физику у Београду, у групи проф. др Радоша Гајића, под ко-менторством др Јелене Пешић.

У октобру 2017. године уписује докторске студије из Физике кондензоване материје и статистичке физике, на Физичком факултету Универзитета у Београду, од када волонтира у Центру за физику чврстог стања и нове материјале, Института за Физику Београд, у Лабораторији за графен, друге 2Д материјале и уређене наноструктуре.

У оквиру свог доктората, Андријана се бави истраживањем особина нових слојевитих и 2Д материјала помоћу аб-инитио прорачуна, на бази теорије функционала густине, под менторством др Јелене Пешић. До сада је коаутор три публикације у међународним часописима, као први аутор једне и други аутор на две публикације.

## Преглед научне активности Андријане Шолајић

Андријана Шолајић се у свом научном раду бави истраживањем особина нових слојевитих и 2Д материјала помоћу ab-initio прорачуна, базираних на теорији функционала густине, са фокусом на електронске особине и динамику решетке оваквих структура. Теорија функционала густине је данас једна од најпопуларнијих унмеричких метода за моделирање материјала, заснована на законима квантне механике. Резултати добијени овим методом се углавном добро слажу са експерименталним резултатима, и користе се како за објашњење и потврду експерименталних резултата, тако и за предвиђање нових материјала и њихових својстава..

Током мастер студија, Андријана је мастер тезу урадила у Центру за чврсто стање Института за физику у Београду, под коменторством др Јелене Пешић. Током изrade мастер тезе бавила се истраживањем електронских и вибрационих особина допиреног графена. Графен, као први прави дводимензиони материјал, поред неизмерне теоријске вредности, отвара могућност за широк спектар примена у различитим областима. Допирање графена је створило могућност за манипулацију његових својстава, при чему је допирање адатомима посебно погодно јер је кристална структура графена у равни очувана, а могуће је постићи висок степен допирања и контролисати Фермијев ниво. У мастер раду, посебно су анализирани ефекти допирања адатомима стронцијума и итербијума, по узору на интеркалирани графит, као и њихов утицај на електронска и вибрациона својства. Показано је како ови допанти мењају електронску и фононску структуру, као и да под њиховим утицајем долази до значајног повећања густине стања на Ферми нивоу. Резултати овог истраживања су објављени у истакнутом међународном часопису.

Током докторских студија, у фокусу истраживачког рада Андријане Шолајић је испитивање особина нових слојевитих и 2Д материјала, путем ab-initio прорачуна. Од оваквих слојевитих материјала, због своје структуре, услед ван дер Валсових веза, ексфолијацијом се лако могу добити монослојеви, што их уз њихова различита својства чини погодним за примене у наноелектроници, оптоелектроници и спинтроници. У досадашњем раду, учествовала је у истраживању два оваква материјала, CrI<sub>3</sub>, из фамилије хром-трихалида, као трихалкогенида CrSiTe<sub>3</sub>, који припадају слојевитим полупроводничким материјалима са феромагнетним уређењем. Андријана је током ових истраживања, уз помоћ теорије функционала густине анализирала вибрациона својства ових структура. Резултати добијени нумеричким прорачунима, показали су добро слагање са експерименталним резултатима добијеним од стране коаутора проистеклих радова и помогли у тумачењу експерименталних резултата. У оквиру истраживања везаног за 2Д материјале, испитивала је механичке и еластичне особине монослоја магнезијум-диборида, који је због својих електричних, као и суперпроводних својстава привукао велику пажњу. Тренутно се бави теоријским разматрањем допирања вишеслојних флексица графена добијених ЛПЕ методом. Андријана Шолајић учествује и у истраживању у оквиру пројекта билатералне сарадње између Србије и Аустрије у периоду 2018-2020. године, на теми "Моделовање и мерење фазних прелаза и оптичких особина код перовскита".

## **Списак публикација Андријане Шолајић**

### **РАДОВИ У ВРХУНСКИМ МЕЂУНАРОДНИМ ЧАСОПИСИМА (М21):**

1. S. Djurdjić-Mijin, A. Šolajić, J. Pešić, M. Šćepanović, Y. Liu, A. Baum, C. Petrović, N. Lazarević, Z.V. Popović, "Lattice dynamics and phase transition in CrI<sub>3</sub> single crystals", Physical Review B 98 (10), 104307 (2018)
2. A. Milosavljević, A. Šolajić, J. Pešić, Yu Liu, C. Petrović, N. Lazarević, Z.V. Popović, "Evidence of spin-phonon coupling in CrSiTe<sub>3</sub>", Physical Review B 98 (10), 104306 (2018)

### **РАДОВИ У ИСТАКНУТИМ МЕЂУНАРОДНИМ ЧАСОПИСИМА (М22):**

3. A. Šolajić, J. Pešić, R. Gajić, "Ab-initio calculations of electronic and vibrational properties of Sr and Yb intercalated graphene", Optical and Quantum Electronics 50 (7), 276 (2018)

### **САОПШТЕЊЕ СА МЕЂУНАРОДНОГ СКУПА ШТАМПАНО У ИЗВОДУ М34:**

1. A. Šolajić, J. Pešić, R. Gajić, "Ab-initio calculations of electronic and vibrational properties of Sr and Yb-intercalated graphene", VI International School and Conference on Photonics - PHOTONICA 2017, 28.8 - 1.9.2017, Beograd, Srbija, ISBN 978-86-82441-46-5
2. A. Šolajić, J. Pešić, R. Gajić, "First principle study of Yb and Sr doped monolayer graphene", Program and the Book of Abstracts / Sixteenth Young Researchers' Conference Materials Sciences and Engineering, December 6-8, 2017, Beograd, Srbija, str 27., ISBN 978-86-80321-33-2



Република Србија  
Универзитет у Београду  
Физички факултет  
Д.Бр.2017/8005  
Датум: 15.10.2018. године

На основу члана 161 Закона о општем управном поступку и службене евиденције издаје се

## УВЕРЕЊЕ

**Шолајић (Слободан) Андријана**, бр. индекса 2017/8005, рођена 05.05.1991. године, Београд, Београд-Савски Венац, Република Србија, уписана школске 2018/2019. године, у статусу: финансирање из буџета; тип студија: докторске академске студије; студијски програм: Физика.

Према Статуту факултета студије трају (број година): три.

Рок за завршетак студија: у двоструком трајању студија.

Ово се уверење може употребити за регулисање војне обавезе, издавање визе, права на дечији додатак, породичне пензије, инвалидског додатка, добијања здравствене књижице, легитимације за повлашћену вожњу и стипендије.

Овлашћено лице факултета



*М. М. Симоновић*



Универзитет у Београду  
Електротехнички факултет  
Број индекса: 2010/0056  
Број: О2015027  
Датум: 03.06.2016.

На основу члана 161 Закона о општем управном поступку ("Службени лист СРЈ", бр. 33/97, 31/2001 и "Службени гласник РС", бр. 30/2010) и службене евиденције, Универзитет у Београду - Електротехнички факултет, издаје

## УВЕРЕЊЕ

*Андрејана Шолајић*

име једног родитеља Слободан, ЈМБГ 0505991715104, рођена 05.05.1991. године, Београд, општина Београд-Савски Венац, Република Србија, уписана школске 2010/11. године, дана 03.06.2016. године завршила је основне академске студије на студијском програму Електротехника и рачунарство, модул Физичка електроника - смер Наноелектроника, оптоелектроника и ласерска техника, у трајању од четири године, обима 240 (двеста четрдесет) ЕСПБ бодова, са просечном оценом 8,26 (осам и 26/100).

На основу наведеног издаје јој се ово уверење о стеченом високом образовању и стручном називу дипломирани инжењер електротехнике и рачунарства.

Декан

Проф. др Зоран Јовановић



Универзитет у Београду  
Електротехнички факултет  
Број индекса: 2016/3129  
Број: М2016074  
Датум: 11.09.2017.

На основу члана 29. Закона о општем управном поступку ("Сл. гласник РС", бр.18/2016) и службене евиденције, Универзитет у Београду - Електротехнички факултет, издаје

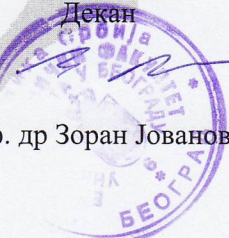
## УВЕРЕЊЕ

*Андијана Шолајић*

име једної родитеља Слободан, ЈМБГ 0505991715104, рођена 05.05.1991. године, Београд, општина Београд-Савски Венац, Република Србија, уписане школске 2016/17. године, дана 07.09.2017. године завршила је мастер академске ступње на студијском програму Електротехника и рачунарство, модул Наноелектроника и фотоника, у трајању од једне године, обима 60 (шездесет) ЕСПБ бодова, са просечном очевом 10,00 (десет и 00/100).

На основу наведеног издаје јој се ово уверење о стеченом високом образовању и академском називу **мастер инжењер електротехнике и рачунарства**.

Проф. др Зоран Јовановић





Република Србија  
Универзитет у Београду  
Електротехнички факултет  
Број индекса: 2010/0056  
Датум: 03.06.2016.

На основу члана 161 Закона о општем управном поступку и службене евиденције издаје се

## УВЕРЕЊЕ О ПОЛОЖЕНИМ ИСПИТИМА

Андиријана Шолајић, име једног родитеља Слободан, ЈМБГ 0505991715104, рођена 05.05.1991. године, Београд, општина Београд-Савски Венац, Република Србија, уписана школске 2010/11. године, дана 03.06.2016. године завршила је основне академске студије на студијском програму Електротехника и рачунарство, модул Физичка електроника - смер Наноелектроника, оптоелектроника и ласерска техника, у трајању од четири године, обима 240 (двеста четрдесет) ЕСПБ бодова, и стекла стручни назив дипломирани инжењер електротехнике и рачунарства. Током студија положила је испите из следећих предмета:

Р.бр.	Шифра	Назив предмета	Оцена	ЕСПБ	Фонд часова**	Датум
1.	ОО1П1	Програмирање 1	7 (седам)	5	I:(45+30+0)	09.02.2011.
2.	ОО1ОЕ1	Основи електротехнике 1	7 (седам)	7	I:(45+45+0)	28.08.2011.
3.	ОО1ЛФ	Лабораторијске вежбе из Физике	10 (десет)	2	I:(0+0+30)	10.01.2011.
4.	ОО1ЕЈ1	Енглески језик 1	10 (десет)	2	I:(30+0+0)	14.01.2011.
5.	ОО1ММ1	Математика 1	8 (осам)	7	I:(45+45+0)	15.01.2011.
6.	ОО1ПКР	Практикум из коришћења рачунара	10 (десет)	2	I:(15+0+15)	21.01.2011.
7.	ОО1Ф1	Физика 1	8 (осам)	5	I:(45+30+0)	02.02.2011.
8.	ОО1ПФ2	Практикум из Физике 2	10 (десет)	2	II:(0+0+30)	06.06.2011.
9.	ОО1ЕЈ2	Енглески језик 2	10 (десет)	2	II:(30+0+0)	13.06.2011.
10.	ОО1ЛОЕ	Лабораторијске вежбе из Основа електротехнике	8 (осам)	2	II:(7,5+0+22,5)	16.06.2011.
11.	ОО1П2	Програмирање 2	7 (седам)	5	II:(45+30+0)	06.07.2011.
12.	ОО1ОЕ2	Основи електротехнике 2	6 (шест)	7	II:(45+45+0)	01.09.2012.
13.	ОО1ММ2	Математика 2	6 (шест)	7	II:(45+45+0)	17.09.2011.
14.	ОО1Ф2	Физика 2	7 (седам)	5	II:(45+30+0)	09.02.2012.
15.	ОФ2ТЕК	Теорија електричних кола	6 (шест)	6	III:(45+30+0)	18.09.2012.
16.	ОФ2ПРМ	Практикум из рачунарских алата у математици	10 (десет)	3	III:(15+0+15)	22.01.2012.
17.	ОФ2ЕЕ	Елементи електронике	6 (шест)	6	III:(45+30+15)	11.09.2013.
18.	ОФ2М3	Математика 3	6 (шест)	6	III:(45+45+0)	09.06.2013.
19.	ОФ2ЕЈ3	Енглески језик 3	10 (десет)	3	III:(30+0+0)	13.01.2012.
20.	ОФ2МУЕ	Материјали у електротехници	9 (девет)	6	III:(45+30+15)	10.01.2012.
21.	ОФ2КМ	Квантна механика	6 (шест)	6	IV:(45+30+0)	08.06.2012.
22.	ОФ2СИС	Сигнали и системи	7 (седам)	6	IV:(45+15+15)	23.09.2012.
23.	ОФ2ОДЕ	Основи дигиталне електронике	6 (шест)	6	IV:(45+15+15)	06.06.2012.
24.	ОФ2ВИС	Вероватноћа и статистика	7 (седам)	3	IV:(15+15+7,5)	05.06.2012.
25.	ОФ2ПКЕ	Практикум из конструисања електронских уређаја	10 (десет)	3	IV:(15+0+22,5)	15.06.2012.
26.	ОФ2ДИФ	Диференцијалне једначине	10 (десет)	3	IV:(15+15+7,5)	26.08.2012.
27.	ОФ2ПСА	Практикум из софтверских алата	6 (шест)	3	IV:(15+0+22,5)	17.06.2012.
28.	ОФ3СФ	Статистичка физика	8 (осам)	6	V:(45+30+0)	24.01.2016.
29.	ОФ3ФЕЧ	Физичка електроника чврстог тела	10 (десет)	6	V:(45+30+0)	17.01.2016.





Република Србија  
Универзитет у Београду  
Електротехнички факултет  
Број индекса: 2010/0056  
Датум: 03.06.2016.

Р.бр.	Шифра	Назив предмета	Оцена	ЕСПБ	Фонд часова**	Датум
30.	ОФЗОБ	Основи биофизике	6 (шест)	6	V:(45+30+0)	15.01.2013.
31.	ОФЗЕЕУ	Елементи електронских уређаја	10 (десет)	6	V:(45+15+15)	10.01.2013.
32.	ОФЗФТМ	Физичко техничка мерења	8 (осам)	6	V:(45+0+30)	21.01.2013.
33.	ОФ4МК	Микроелектронска кола	10 (десет)	6	VI:(45+30+0)	05.07.2013.
34.	ОФ3МИН	Микроелектроника и наноелектроника	6 (шест)	6	VI:(45+30+0)	22.08.2013.
35.	ОФ3О	Оптоелектроника	6 (шест)	6	VI:(45+15+15)	11.06.2015.
36.	ОФ3СП	Сензори и претварачи	8 (осам)	6	VI:(45+0+30)	06.09.2013.
37.	ОФ3ПМК	Примена микроконтролера	10 (десет)	6	VI:(45+30+0)	08.06.2013.
38.	ОФ4ПЛМ	Примена ласера у медицини	10 (десет)	6	VII:(45+30+0)	19.09.2014.
39.	ОФ4ФС	Фiberоптички сензори	9 (девет)	6	VII:(45+15+15)	15.09.2014.
40.	ОФ4АМП	Анализа и моделовање полупроводничких направа	10 (десет)	6	VII:(45+30+0)	13.01.2014.
41.	ОФ4ПКН	Полупроводничке квантне наноструктуре	10 (десет)	6	VII:(45+30+0)	24.08.2015.
42.	ОФ4ЛТ	Ласерска техника	10 (десет)	6	VII:(45+30+0)	23.08.2014.
43.	ОФ4НАН	Наноелектронске направе	8 (осам)	6	VIII:(45+30+0)	24.08.2015.
44.	ОФ4МЕС	Микроелектромеханички системи	9 (девет)	6	VIII:(45+30+0)	01.09.2015.
45.	ОФ4ОЛС	Оптоелектронски и лазерски мерни системи	9 (девет)	6	VIII:(45+0+30)	19.08.2014.

\* - еквивалентиран/признат испит.

\*\* - Фонд часова је у формату (предавања+вежбе+остало).

Одрађене обавезе:

Р.бр.	Назив обавезе	ЕСПБ
1.	Стручна пракса	2

Укупно остварено 240 ЕСПБ.

Општи успех: 8,26 (осам и 26/100), по годинама студија (8,14, 7,62, 8,20, 9,38).

Завршни рад одбрањен је дана 03.06.2016. године са оценом 10 (десет).





Република Србија  
Универзитет у Београду  
Електротехнички факултет  
Број индекса: 2016/3129  
Датум: 11.09.2017.

На основу члана 29. Закона о општем управном поступку и службене евиденције издаје се

## УВЕРЕЊЕ О ПОЛОЖЕНИМ ИСПИТИМА

Андрјана Шолајић, име једног родитеља Слободан, ЈМБГ 0505991715104, рођена 05.05.1991. године, Београд, општина Београд-Савски Венац, Република Србија, уписана школске 2016/17. године, дана 07.09.2017. године завршила је мастер академске студије на студијском програму Електротехника и рачунарство, модул Наноелектроника и фотоника, у трајању од једне године, обима 60 (шездесет) ЕСПБ бодова, и стекла академски назив мастер инжењер електротехнике и рачунарства. Током студија положила је испите из следећих предмета:

Р.бр.	Шифра	Назив предмета	Оцена	ЕСПБ	Фонд часова**	Датум
1.	13M061ЕНН	Елементи нанооптике и нанофотонике	10 (десет)	6	I:(45+15+0)	14.02.2017.
2.	13M061ДНКС	Дизајн наноелектронских квантних структура	10 (десет)	6	I:(60+0+0)	13.02.2017.
3.	13M061МНР	Методологија научног рада	10 (десет)	6	I:(60+0+0)	24.01.2017.
4.	13M061ММН	Моделовање микроелектронских направа	10 (десет)	6	I:(45+15+0)	24.01.2017.
5.	13M061НИН	Наномагнетизам и наноспинtronика	10 (десет)	6	I:(45+15+0)	17.01.2017.

\* - еквивалентиран/признат испит.

\*\* - Фонд часова је у формату (предавања+вежбе+остало).

Начин оцењивања на предметима:

Оцена	Значење оцене	Број поена	
		од	до
10	одличан	91	100
9	изузетно добар	81	90
8	врло добар	71	80
7	добар	61	70
6	довољан	51	60

Укупно остварено 60 ЕСПБ.

Општи успех: 10,00 (десет и 00/100)

Завршни - мастер рад одбрањен је дана 07.09.2017. године са оценом 10 (десет).

Шеф Студентског одсека

Драгана Треневски Виденов



Република Србија  
Универзитет у Београду  
Физички факултет  
Број индекса: 2017/8005  
Датум: 04.10.2018.

На основу члана 29. Закона о општем управном поступку и службене евиденције издаје се

## УВЕРЕЊЕ О ПОЛОЖЕНИМ ИСПИТИМА

Андрјана Шолајић, име једног родитеља Слободан, рођена 05.05.1991. године, Београд, Београд-Савски Венац, Република Србија, уписана школске 2017/2018. године на докторске академске студије, школске 2017/2018. године уписана на статус финансирање из буџета, студијски програм Физика, током студија положила је испите из следећих предмета:

Р.бр.	Шифра	Назив предмета	Оцена	ЕСПБ	Фонд часова**	Датум
1.	ДС15КМ16	Компјутерско моделовање структурних и електронских особина материјала	10 (десет)	15	I:(8+0+0)	21.08.2018.
2.	ДС15КМ17	Скенирајућа атомска микроскопија чврстих тела	10 (десет)	15	II:(8+0+0)	24.08.2018.
3.	ДС15ФРНД1	Рад на докторату I. део	П.	30	I:(0+0+12) II:(0+0+12)	

\* - еквивалентиран/признат испит.

\*\* - Фонд часова је у формату (предавања+вежбе+остало).

Општи успех: 10,00 (десет и 00/100), по годинама студија (10,00, /, /).

Овлашћено лице факултета

М. Маселић





## Evidence of spin-phonon coupling in CrSiTe<sub>3</sub>

A. Milosavljević,<sup>1</sup> A. Šolajić,<sup>1</sup> J. Pešić,<sup>1</sup> Yu Liu (刘育),<sup>2</sup> C. Petrović,<sup>2</sup> N. Lazarević,<sup>1,\*</sup> and Z. V. Popović<sup>1,3</sup>

<sup>1</sup>*Center for Solid State Physics and New Materials, Institute of Physics Belgrade,  
University of Belgrade, Pregrevica 118, 11080 Belgrade, Serbia*

<sup>2</sup>*Condensed Matter Physics and Materials Science Department, Brookhaven National Laboratory, Upton, New York 11973-5000, USA*

<sup>3</sup>*Serbian Academy of Sciences and Arts, Knez Mihailova 35, 11000 Belgrade, Serbia*



(Received 12 July 2018; published 18 September 2018)

We present Raman scattering results on the layered semiconducting ferromagnetic compound CrSiTe<sub>3</sub>. Four Raman-active modes, predicted by symmetry, are observed and assigned. The experimental results are supported by density functional theory calculations. The self-energies of the  $A_g^3$  and the  $E_g^3$  symmetry modes exhibit unconventional temperature evolution around 180 K. In addition, the doubly degenerate  $E_g^3$  mode shows a clear change of asymmetry in the same temperature region. The observed behavior is consistent with the presence of the previously reported short-range magnetic order and strong spin-phonon coupling.

DOI: [10.1103/PhysRevB.98.104306](https://doi.org/10.1103/PhysRevB.98.104306)

### I. INTRODUCTION

Trichalcogenides CrXTe<sub>3</sub> ( $X = \text{Si, Ge}$ ) belong to a rare class of quasi-two-dimensional semiconducting materials with a ferromagnetic order, band gaps of 0.4 eV for Si and 0.7 eV for Ge compounds, and Curie temperatures ( $T_C$ ) of 32 and 61 K, respectively [1–6]. Because of their layered structure, due to van der Waals bonding, they can be exfoliated to mono- and few-layer nanosheets, which, together with their semiconducting and magnetic properties, make an ideal combination for applications in optoelectronics and nanospintrronics [7–11]. This was further supported by the observation of giant resistivity modulation of CrGeTe<sub>3</sub>-based devices [12].

From an x-ray diffraction study [1], it was revealed that CrSiTe<sub>3</sub> crystals are twinned along  $c$  axes, the thermal expansion is negative at low temperatures, and the thermal conductivity shows strong magnon-phonon scattering effects. A very small single-ion anisotropy favoring magnetic order along  $c$  axes and spin waves was found in CrSiTe<sub>3</sub> by elastic and inelastic neutron scattering [13]. Spin-wave measurements suggest the absence of three-dimensional correlations above  $T_C$ , whereas in-plane dynamic correlations are present up to 300 K. First-principles calculations suggested the possibility of graphenelike mechanical exfoliation for CrXTe<sub>3</sub> ( $X = \text{Si, Ge}$ ) single crystals with conserved semiconducting and ferromagnetic properties [14]. The exfoliation of CrSiTe<sub>3</sub> bulk to mono- and few-layer two-dimensional crystals onto a Si/SiO<sub>2</sub> substrate has been achieved [15] with a resistivity between 80 and 120 K, depending on the number of layers. Critical exponents for CrSiTe<sub>3</sub> were also determined from theoretical analysis [16].

Spin-phonon coupling in CrGeTe<sub>3</sub> was investigated in Raman scattering experiments [17]. Splitting of the two lowest-energy  $E_g$  modes in the ferromagnetic phase has been observed and ascribed to time-reversal symmetry breaking by

the spin ordering. Furthermore, the significant renormalization of the three higher-energy modes' self-energies below  $T_C$  provided additional evidence of spin-phonon coupling [17]. The external pressure-induced effect on lattice dynamics and magnetization in CrGeTe<sub>3</sub> has also been studied [18].

The Raman spectrum of CrSiTe<sub>3</sub> single crystals was reported in Ref. [1], where three Raman-active modes have been observed. Similar results have also been presented in Ref. [15] for ultrathin nanosheets of CrSiTe<sub>3</sub>. Here, we report a Raman scattering study of CrSiTe<sub>3</sub> single crystals, with the main focus on phonon properties in the temperature range between 100 and 300 K. Our experimental results are qualitatively different from those previously reported [1,15] but consistent with the results obtained for CrGeTe<sub>3</sub> [17,18]. Furthermore, our data reveal the asymmetry of the  $E_g^3$  mode, which is suppressed at higher temperatures. The  $A_g^3$  and  $E_g^3$  symmetry modes exhibit nonanharmonic self-energy temperature dependence in the region around 180 K, related to the strong spin-lattice interaction due to short-range magnetic order [1]. Energies and symmetries of the observed Raman-active modes are in good agreement with theoretical calculations.

### II. EXPERIMENT AND NUMERICAL METHOD

Single crystals of CrSiTe<sub>3</sub> and CrGeTe<sub>3</sub> were grown as described previously [19]. For a Raman scattering experiment, a Tri Vista 557 spectrometer was used in the backscattering micro-Raman configuration with a 1800/1800/2400 grooves/mm diffraction grating combination. A coherent Verdi G solid-state laser with a 532-nm line was used as the excitation source. The direction of the incident (scattered) light coincides with a crystallographic  $c$  axis. Right before being placed in the vacuum, the samples were cleaved in the air. All measurements were performed in a high vacuum ( $10^{-6}$  mbar) using a KONTI CryoVac continuous-helium-flow cryostat with a 0.5-mm-thick window. Laser-beam focusing was achieved through a microscope objective with  $\times 50$  magnification, a spot size of approximately 8  $\mu\text{m}$ , and a power

\*nenadl@ipb.ac.rs

TABLE I. Calculated and experimental crystallographic lattice parameters for  $\text{CrSiTe}_3$  ( $|a| = |b|$ ), bond lengths, interlayer distance ( $d$ ), and van der Waals (vdW) gap.

$\text{CrSiTe}_3$	Calculation (Å)	Experiment (Å) [20]
$a$	6.87	6.76
$c$	19.81	20.67
Si-Si	2.27	2.27
Si-Te	2.52	2.51
Cr-Te	2.77	2.78
$d$	6.86	6.91
vdW gap	3.42	3.42

<2 mW on the surface of a sample. All spectra were corrected for the Bose factor.

Density functional theory calculations were performed in the Quantum Espresso software package [21], using the PBE exchange-correlation functional [22], PAW pseudopotentials [23,24], and energy cutoffs for wave functions and the charge density of 85 and 425 Ry, respectively. For  $k$ -point sampling, the Monkhorst-Pack scheme was used, with a  $\Gamma$ -centered  $8 \times 8 \times 8$  grid. Optimization of the atomic positions in the unit cell was performed until the interatomic forces were minimized down to  $10^{-6}$  Ry/Å. In order to obtain the parameters accurately, treatment of the van der Waals interactions was included using the Grimme-D2 correction [25]. Phonon frequencies were calculated at the  $\Gamma$  point

within the linear response method implemented in Quantum Espresso. Calculated crystallographic properties obtained by relaxing the structures are in good agreement with x-ray diffraction measurements [20]. A comparison between our, calculated, and experimental results is presented in Table I.

### III. RESULTS AND DISCUSSION

#### A. Polarization dependence

$\text{CrSiTe}_3$  crystallizes in the rhombohedral crystal structure, described by  $R\bar{3}$  ( $C_{3i}^2$ ) [26]. Wyckoff positions of atoms, together with each site's contribution to phonons at the  $\Gamma$  point and corresponding Raman tensors, are listed in Table II. The phonon mode distribution obtained by factor-group analysis for the  $R\bar{3}$  space group is as follows:

$$\begin{aligned}\Gamma_{\text{Raman}} &= 5A_g + 5E_g, \\ \Gamma_{\text{IR}} &= 4A_u + 4E_u, \\ \Gamma_{\text{Acoustic}} &= A_u + E_u.\end{aligned}$$

Since the plane of incidence is  $ab$ , where  $|a| = |b|$  [ $\angle(a, b) = 120^\circ$ ], and the direction of light propagation is along  $c$  axes, from the selection rules, it is possible to observe all Raman-active modes, i.e., five  $A_g$  modes and five doubly degenerate  $E_g$  modes. According to the Raman tensors presented in Table II,  $A_g$  symmetry modes are observable only in the parallel polarization configuration, whereas  $E_g$  symmetry

TABLE II. (a) Type of atoms, Wyckoff positions, each site's contribution to the phonons at the  $\Gamma$  point, and corresponding Raman tensors for the  $R\bar{3}$  space group of  $\text{CrSiTe}_3$ . (b) Phonon symmetry, calculated optical phonon frequencies at 0 K, and experimental values for Raman-active (at 100 K) and infrared (IR)-active (at 110 K) [1]  $\text{CrSiTe}_3$  phonons.

(a) Space group $R\bar{3}$ (No. 148)					
Atom(s) (Wyckoff positions)			Irreducible representations		
Cr, Si (6c)			$A_g + E_g + A_u + E_u$		
Te (18f)			$3A_g + 3E_g + 3A_u + 3E_u$		
(b) Raman tensors					
$A_g = \begin{pmatrix} a & 0 & 0 \\ 0 & b & 0 \\ 0 & 0 & c \end{pmatrix}$	$E_g^1 = \begin{pmatrix} c & d & e \\ d & -c & f \\ e & f & 0 \end{pmatrix}$		$E_g^2 = \begin{pmatrix} d & -c & -f \\ -c & -d & e \\ -f & e & 0 \end{pmatrix}$		
Raman active					
Symmetry	Calc. (cm <sup>-1</sup> )	Expt. (cm <sup>-1</sup> )	Symmetry	Calc. (cm <sup>-1</sup> )	Expt. (cm <sup>-1</sup> )
$A_g^1$	88.2	—	$A_u^1$	91.8	91.0
$E_g^1$	93.5	88.9	$E_u^1$	93.7	—
$E_g^2$	96.9	—	$A_u^2$	116.8	—
$E_g^3$	118.3	118.2	$E_u^2$	117.1	—
$A_g^2$	122.0	—	$A_u^3$	202.4	—
$A_g^3$	148.0	147.4	$E_u^3$	206.2	207.9
$A_g^4$	208.7	—	$A_u^4$	243.7	—
$E_g^4$	219.5	217.2	$E_u^4$	365.8	370.4
$E_g^5$	357.4	—			
$A_g^5$	508.8	—			

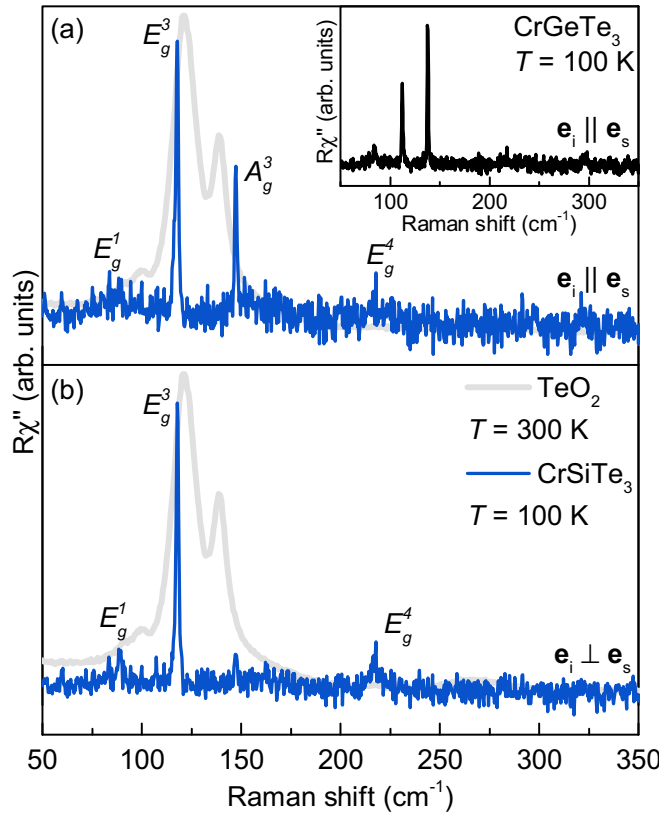


FIG. 1. Raman spectra of CrSiTe<sub>3</sub> single crystals measured at 100 K in (a) parallel and (b) cross polarization configurations. The gray line represents the TeO<sub>2</sub> spectrum measured at 300 K. Inset: Raman spectrum of CrGeTe<sub>3</sub> in the parallel polarization configuration measured at 100 K.

modes can be expected to appear for both in-parallel and cross polarization configurations.

The Raman spectra of CrSiTe<sub>3</sub> for two main linear polarization configurations, at 100 K, are shown in Fig. 1. Four peaks can be observed in the spectra, at energies of 88.9, 118.2, 147.4, and 217.2 cm<sup>-1</sup>. Since only the peak at 147.4 cm<sup>-1</sup> vanishes in the cross polarization configuration, it corresponds to the A<sub>g</sub> symmetry mode. The other three modes appear in both parallel and cross polarization configurations and, thereby, can be assigned as E<sub>g</sub> symmetry modes (Fig. 1).

In order to exclude the possibility that any of the observed features originate from the TeO<sub>2</sub> [17,27], its Raman spectrum is also presented in Fig. 1. It can be noted that no TeO<sub>2</sub> contribution is present in our CrSiTe<sub>3</sub> data. Furthermore, the observed CrSiTe<sub>3</sub> Raman spectra are also consistent with the CrGeTe<sub>3</sub> Raman spectra (see inset in Fig. 1), isostructural to CrSiTe<sub>3</sub>. Five Raman-active modes have been observed for CrGeTe<sub>3</sub>, two A<sub>g</sub> modes, at 137.9 and 296.6 cm<sup>-1</sup>, and three E<sub>g</sub> modes, at 83.5, 112.2, and 217.5 cm<sup>-1</sup>, in agreement with the previously published data [17,18]. The main difference in the spectra of CrSiTe<sub>3</sub> and CrGeTe<sub>3</sub> arises from the change in mass and lattice parameter effects that cause the peaks to shift.

Calculated and observed Raman-active phonon energies are compiled in Table II, together with the experimental energies of the infrared (IR)-active phonons [1], and are found to be in good agreement. Displacement patterns of the A<sub>g</sub>

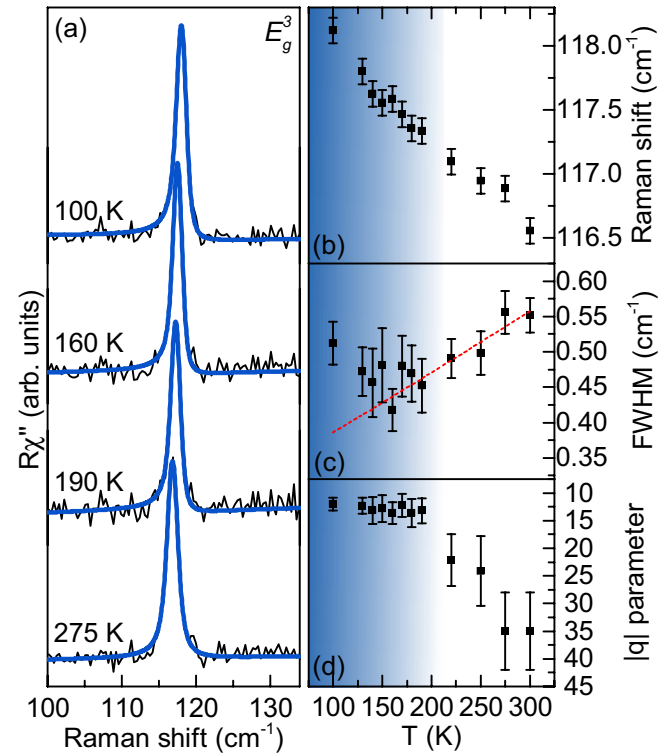


FIG. 2. (a) The  $E_g^3$  mode Raman spectra of CrSiTe<sub>3</sub> at four temperatures measured in the cross polarization configuration. Blue lines represent line shapes obtained as a convolution of the Fano line shape and Gaussian, calculated to fit the experimental data. Temperature dependence of (b) the energy, (c) the line width, and (d) the Fano parameter  $q$  of the  $E_g^3$  mode. The dashed red line represents standard anharmonic behavior [28,29]. All the parameters show a change in tendency around 180 K.

and  $E_g$  symmetry modes are presented in Fig. 4, in the Appendix.

## B. Temperature dependence

After proper assignment of all the observed CrSiTe<sub>3</sub> Raman-active modes we proceeded with temperature evolution of their properties, focusing on the most prominent ones,  $E_g^3$  and  $A_g^3$ . Figure 2(a) shows the spectral region of the doubly degenerate  $E_g^3$  mode at an energy of 118.2 cm<sup>-1</sup>, at four temperatures. Closer inspection of the 100 K spectra revealed clear asymmetry of the peak on the low-energy side. The presence of defects may result in the appearance of the mode asymmetry [30], however, they would also contribute to the mode line width and, possibly, the appearance of phonons from the edge of the Brillouin zone in the Raman spectra [29]. The very narrow lines and absence of additional features in the Raman spectra of CrSiTe<sub>3</sub> do not support this scenario. The asymmetry may also arise when the phonon is coupled to a continuum [31]. Such a coupling of the  $E_g^3$  phonon mode would result in a line shape given by the convolution of a Fano function and a Gaussian, the latter representing the resolution of the spectrometer [29]. Comparison between the Fano line shape convoluted with a Gaussian, the Voigt line shape, and the experimental data at 100 K is presented in Fig. 5, in the

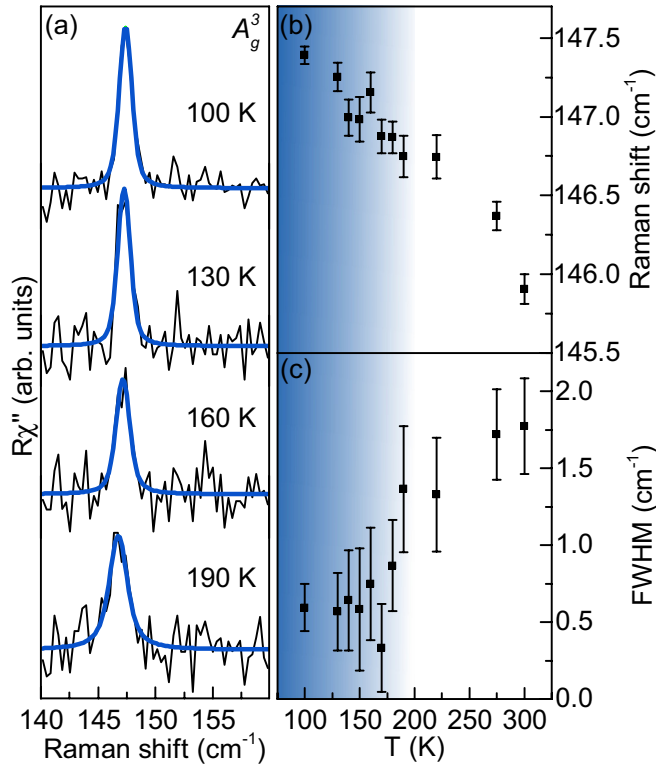


FIG. 3. (a)  $A_g^3$  mode Raman spectra of  $\text{CrSiTe}_3$  at four temperatures measured in the parallel polarization configuration. Blue lines represent Voigt line shapes. (b) Energy and (c) line-width temperature dependence of the  $A_g^3$  mode.

Appendix, with the former yielding better agreement with the experimental data. Furthermore, it fully captures the  $E_g^3$  mode line shape at all temperatures under investigation [Figs. 2(a) and 6].

Upon cooling of the sample, the  $E_g^3$  mode energy hardens [Fig. 2(b)] with a very small discontinuity in the temperature range around 180 K. Down to the same temperature, the line width monotonically narrows in line with the standard anharmonic behavior [dashed red line in Fig. 2(c)]. Upon further cooling, the line width increased, deviating from the expected anharmonic tendency. This indicates activation of an additional scattering mechanism, e.g., spin-phonon interaction. Figure 2(d) shows the evolution of the Fano parameter,  $|q|$ . Whereas in the region below 180 K, it increases slightly but continuously, at higher temperatures it promptly goes to lower values and the mode recovers a symmetric line shape. We believe that the observed behavior of the  $E_g^3$  mode can be traced back to the short-range magnetic correlations, which, according to Ref. [1], persist up to 150 K, and the strong spin-phonon coupling in  $\text{CrSiTe}_3$ . Similar behavior of the energy and line width, which differs from the conventional anharmonic, as well as the  $E_g$  mode Fano-type line shape, was recently reported in  $\alpha\text{-RuCl}_3$  and was interpreted as a consequence of the spin-phonon interaction [32].

Unlike the  $E_g^3$  mode, no pronounced asymmetry was observed for the  $A_g^3$  mode. As can be seen from Figs. 3(b) and 3(c) both the energy and the line width of the  $A_g^3$  mode showed

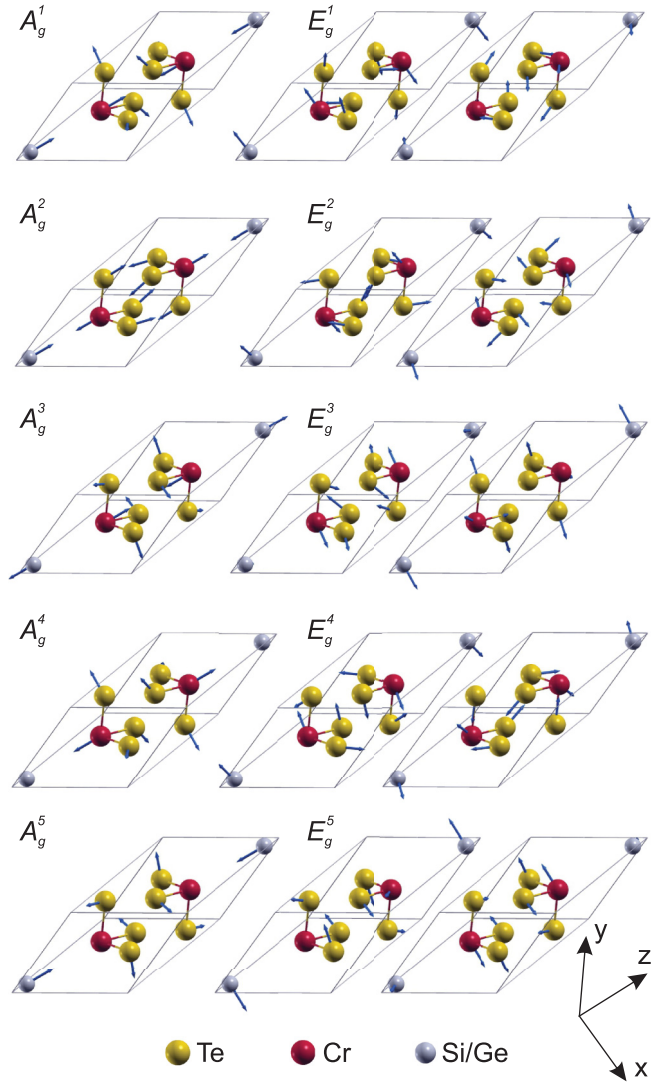


FIG. 4. Unit cell of a  $\text{CrSiTe}_3$  single crystal (solid lines) with the displacement patterns of the  $A_g$  and  $E_g$  symmetry modes. Arrow lengths are proportional to the square root of the interatomic forces.

a similar change in tendency in the same temperature region as the  $E_g^3$  mode, most likely due to the spin-phonon coupling.

#### IV. CONCLUSION

The lattice dynamics of  $\text{CrSiTe}_3$ , a compound isostructural to  $\text{CrGeTe}_3$ , is presented. An  $A_g$  and three  $E_g$  modes were observed and assigned. The experimental results are well supported by theoretical calculations. The temperature dependences of the energies and line widths of the  $A_g^3$  and  $E_g^3$  modes deviate from the conventional anharmonic model in the temperature range around 180 K. In addition, the  $E_g^3$  mode shows clear Fano resonance at lower temperatures. This can be related to the previously reported short-range magnetic correlations at temperatures up to 150 K [1] and the strong spin-phonon coupling.

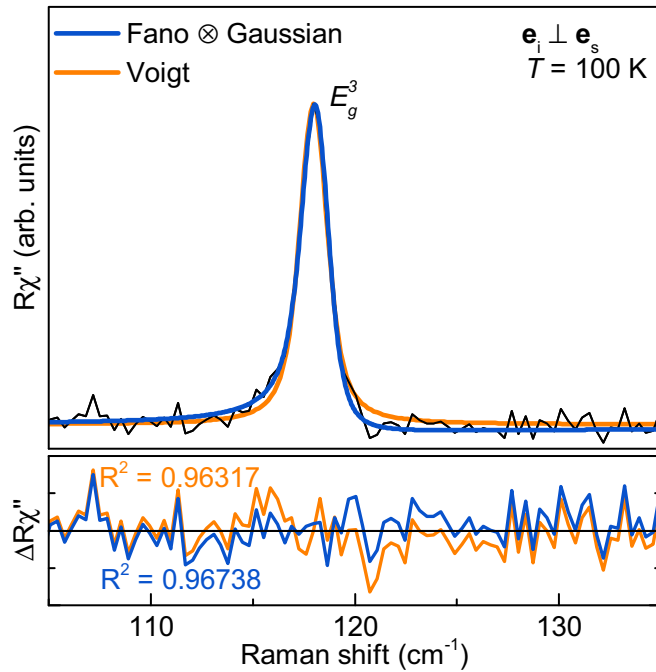


FIG. 5. Analysis of the  $E_g^3$  asymmetry. Measured data are shown as the black line. The solid blue line represents the line shape obtained as a convolution of the Fano line shape and a Gaussian, whereas the orange line represents a Voigt line shape, both calculated to fit the experimental data. The Voigt profile deviates from the experimental data at the peak flanks.

## ACKNOWLEDGMENTS

The work was supported by the Serbian Ministry of Education, Science and Technological Development under Projects III45018 and OI171005. DFT calculations were performed using computational resources at Johannes Kepler University, Linz, Austria. Work at Brookhaven is supported by the U.S. DOE under Contract No. DE-SC0012704.

A.M. and N.L. conceived and performed the experiment, analyzed and discussed data, and wrote the paper; A.S. and J.P. calculated phonon energies, analyzed and discussed data, and wrote the paper; Y.L. and C.P. synthesized and characterized the samples; Z.V.P. analyzed and discussed data and wrote the paper. All authors commented on the manuscript.

## APPENDIX

### 1. Eigenvectors of Raman-active modes

Figure 4 summarizes the  $A_g$  and  $E_g$  symmetry mode displacement patterns of a CrSiTe<sub>3</sub> single crystal ( $R\bar{3}$  space group). Arrow lengths are proportional to the square root of the interatomic forces.

### 2. Asymmetry of the $E_g^3$ line

The peak at  $118.2 \text{ cm}^{-1}$ , which we assigned as the  $E_g^3$  symmetry mode, at low temperatures shows a significant asymmetry towards lower energies. The possibility of additional defect-induced features in Raman spectra can be excluded, since the modes are very narrow, suggesting high crystallinity

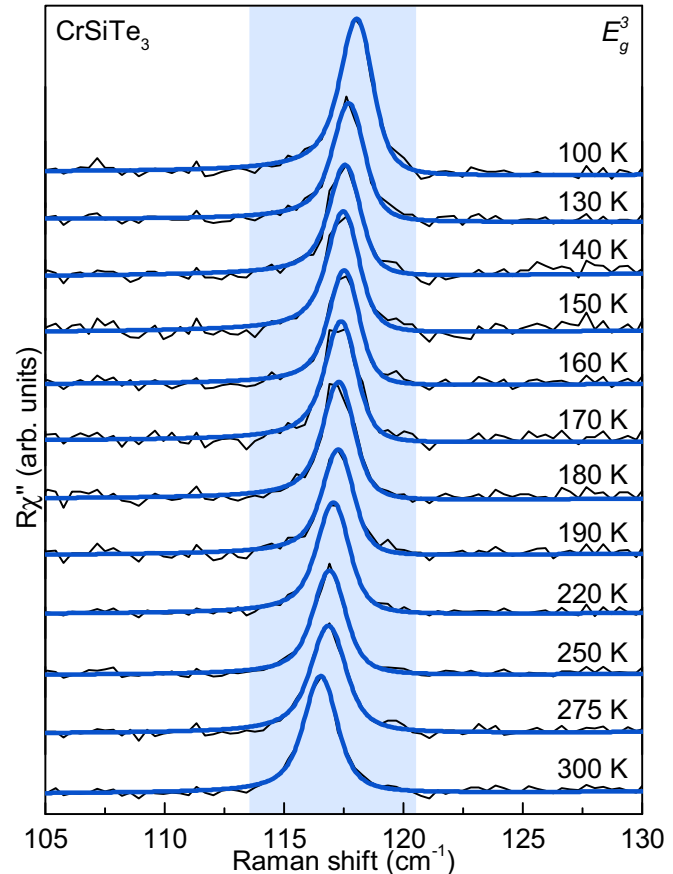


FIG. 6. The  $E_g^3$  mode Raman spectra of CrSiTe<sub>3</sub> at all temperatures measured in the cross polarization configuration. Blue lines represent calculated spectra obtained as the convolution of the Fano line shape and Gaussian.

of the sample. Also, the theoretical calculations do not predict additional Raman-active modes in this energy region. On the other hand, coupling of the phonon mode to a continuum may result in an asymmetric line shape described with the Fano function. Due to the finite resolution of the spectrometer it has to be convoluted with a Gaussian ( $\Gamma_G = 1 \text{ cm}^{-1}$ ). In Fig. 5 we present a comparison of the line obtained as a convolution of the Fano line shape and a Gaussian (blue line) and a Voigt line shape (orange line) fitted to the experimental data. Whereas the Voigt line shape deviates at the peak flanks, excellent agreement has been achieved for convolution of the Fano line shape and a Gaussian.

### 3. $E_g^3$ mode temperature dependence

Figure 6 shows Raman spectra of CrSiTe<sub>3</sub> in the region of the  $E_g^3$  mode in the cross polarization configuration at various temperatures. Solid blue lines represent the convolution of the Fano line shape and Gaussian fitted to the experimental data. The asymmetry is the most pronounced below 190 K. Above this temperature, the asymmetry is decreasing, and at high temperatures the peak recovers the fully symmetric line shape.

- [1] L. D. Casto, A. J. Clune, M. O. Yokosuk, J. L. Musfeldt, T. J. Williams, H. L. Zhuang, M.-W. Lin, K. Xiao, R. G. Hennig, B. C. Sales, J.-Q. Yan, and D. Mandrus, Strong spin-lattice coupling in CrSiTe<sub>3</sub>, *APL Mater.* **3**, 041515 (2015).
- [2] X. Zhang, Y. Zhao, Q. Song, S. Jia, J. Shi, and W. Han, Magnetic anisotropy of the single-crystalline ferromagnetic insulator Cr<sub>2</sub>Ge<sub>2</sub>Te<sub>6</sub>, *Jpn. J. Appl. Phys.* **55**, 033001 (2016).
- [3] T. Leineweber and H. Kronmuller, Micromagnetic examination of exchange coupled ferromagnetic nanolayers, *J. Magn. Magn. Mater.* **176**, 145 (1997).
- [4] G. Ouverard, E. Sandre, and R. Brec, Synthesis and crystal structure of a new layered phase: The chromium hexatellurosilicate Cr<sub>2</sub>Si<sub>2</sub>Te<sub>6</sub>, *J. Solid State Chem.* **73**, 27 (1988).
- [5] B. Siberchicot, S. Jobic, V. Carteaux, P. Gressier, and G. Ouverard, Band structure calculations of ferromagnetic chromium tellurides CrSiTe<sub>3</sub> and CrGeTe<sub>3</sub>, *J. Phys. Chem.* **100**, 5863 (1996).
- [6] V. Carteaux, F. Moussa, and M. Spiesser, 2D Ising-like ferromagnetic behaviour for the lamellar Cr<sub>2</sub>Si<sub>2</sub>Te<sub>6</sub> compound: A neutron scattering investigation, *Europhys. Lett.* **29**, 251 (1995).
- [7] N. Sivadas, M. W. Daniels, R. H. Swendsen, S. Okamoto, and D. Xiao, Magnetic ground state of semiconducting transition-metal trichalcogenide monolayers, *Phys. Rev. B* **91**, 235425 (2015).
- [8] K. S. Novoselov, A. K. Geim, S. V. Morozov, D. Jiang, Y. Zhang, S. V. Dubonos, I. V. Grigorieva, and A. A. Firsov, Electric field effect in atomically thin carbon films, *Science* **306**, 666 (2004).
- [9] Q. H. Wang, K. Kalantar-Zadeh, A. Kis, J. N. Coleman, and M. S. Strano, Electronics and optoelectronics of two-dimensional transition metal dichalcogenides, *Nat. Nanotechnol.* **7**, 699 (2012), review Article.
- [10] C. Gong, L. Li, Z. Li, H. Ji, A. Stern, Y. Xia, T. Cao, W. Bao, C. Wang, Y. Wang, Z. Q. Qiu, R. J. Cava, S. G. Louie, J. Xia, and X. Zhang, Discovery of intrinsic ferromagnetism in two-dimensional van der Waals crystals, *Nature* **546**, 265 (2017).
- [11] B. Huang, G. Clark, E. Navarro-Moratalla, D. R. Klein, R. Cheng, K. L. Seyler, D. Zhong, E. Schmidgall, M. A. McGuire, D. H. Cobden, W. Yao, D. Xiao, P. Jarillo-Herrero, and X. Xu, Layer-dependent ferromagnetism in a van der Waals crystal down to the monolayer limit, *Nature* **546**, 270 (2017).
- [12] W. Xing, Y. Chen, P. M. Odenthal, X. Zhang, W. Yuan, T. Su, Q. Song, T. Wang, J. Zhong, S. Jia, X. C. Xie, Y. Li, and W. Han, Electric field effect in multilayer Cr<sub>2</sub>Ge<sub>2</sub>Te<sub>6</sub>: A ferromagnetic 2D material, *2D Mater.* **4**, 024009 (2017).
- [13] T. J. Williams, A. A. Aczel, M. D. Lumsden, S. E. Nagler, M. B. Stone, J.-Q. Yan, and D. Mandrus, Magnetic correlations in the quasi-two-dimensional semiconducting ferromagnet CrSiTe<sub>3</sub>, *Phys. Rev. B* **92**, 144404 (2015).
- [14] X. Li and J. Yang, CrXTe<sub>3</sub> (X = Si, Ge) nanosheets: Two dimensional intrinsic ferromagnetic semiconductors, *J. Mater. Chem. C* **2**, 7071 (2014).
- [15] M.-W. Lin, H. L. Zhuang, J. Yan, T. Z. Ward, A. A. Puretzky, C. M. Rouleau, Z. Gai, L. Liang, V. Meunier, B. G. Sumpter, P. Ganesh, P. R. C. Kent, D. B. Geohegan, D. G. Mandrus, and K. Xiao, Ultrathin nanosheets of CrSiTe<sub>3</sub>: A semiconducting two-dimensional ferromagnetic material, *J. Mater. Chem. C* **4**, 315 (2016).
- [16] B. Liu, Y. Zou, S. Zhou, L. Zhang, Z. Wang, H. Li, Z. Qu, and Y. Zhang, Critical behavior of the van der Waals bonded high T<sub>C</sub> ferromagnet Fe<sub>3</sub>GeTe<sub>2</sub>, *Sci. Rep.* **7**, 6184 (2017).
- [17] Y. Tian, M. J. Gray, H. Ji, R. J. Cava, and K. S. Burch, Magneto-elastic coupling in a potential ferromagnetic 2D atomic crystal, *2D Mater.* **3**, 025035 (2016).
- [18] Y. Sun, R. C. Xiao, G. T. Lin, R. R. Zhang, L. S. Ling, Z. W. Ma, X. Luo, W. J. Lu, Y. P. Sun, and Z. G. Sheng, Effects of hydrostatic pressure on spin-lattice coupling in two-dimensional ferromagnetic Cr<sub>2</sub>Ge<sub>2</sub>Te<sub>6</sub>, *Appl. Phys. Lett.* **112**, 072409 (2018).
- [19] Y. Liu and C. Petrovic, Critical behavior of quasi-two-dimensional semiconducting ferromagnet Cr<sub>2</sub>Ge<sub>2</sub>Te<sub>6</sub>, *Phys. Rev. B* **96**, 054406 (2017).
- [20] G. T. Lin, H. L. Zhuang, X. Luo, B. J. Liu, F. C. Chen, J. Yan, Y. Sun, J. Zhou, W. J. Lu, P. Tong, Z. G. Sheng, Z. Qu, W. H. Song, X. B. Zhu, and Y. P. Sun, Tricritical behavior of the two-dimensional intrinsically ferromagnetic semiconductor CrGeTe<sub>3</sub>, *Phys. Rev. B* **95**, 245212 (2017).
- [21] P. Giannozzi, S. Baroni, N. Bonini, M. Calandra, R. Car, C. Cavazzoni, D. Ceresoli, G. L. Chiarotti, M. Cococcioni, I. Dabo, A. D. Corso, S. de Gironcoli, S. Fabris, G. Fratesi, R. Gebauer, U. Gerstmann, C. Gougoussis, A. Kokalj, M. Lazzeri, L. Martin-Samos, N. Marzari, F. Mauri, R. Mazzarello, S. Paolini, A. Pasquarello, L. Paulatto, C. Sbraccia, S. Scandolo, G. Sclauzero, A. P. Seitsonen, A. Smogunov, P. Umari, and R. M. Wentzcovitch, Quantum espresso: A modular and open-source software project for quantum simulations of materials, *J. Phys.: Condens. Matter* **21**, 395502 (2009).
- [22] J. P. Perdew, K. Burke, and M. Ernzerhof, Generalized Gradient Approximation Made Simple, *Phys. Rev. Lett.* **77**, 3865 (1996).
- [23] P. E. Blöchl, Projector augmented-wave method, *Phys. Rev. B* **50**, 17953 (1994).
- [24] G. Kresse and D. Joubert, From ultrasoft pseudopotentials to the projector augmented-wave method, *Phys. Rev. B* **59**, 1758 (1999).
- [25] G. Stefan, Semiempirical GGA-type density functional constructed with a long-range dispersion correction, *J. Comput. Chem.* **27**, 1787 (2006).
- [26] R. E. Marsh, The crystal structure of Cr<sub>2</sub>Si<sub>2</sub>Te<sub>6</sub>: Corrigendum, *J. Solid State Chem.* **77**, 190 (1988).
- [27] N. Lazarević, E. S. Bozin, M. Šćepanović, M. Opačić, Hechang Lei, C. Petrović, and Z. V. Popović, Probing IrTe<sub>2</sub> crystal symmetry by polarized Raman scattering, *Phys. Rev. B* **89**, 224301 (2014).
- [28] M. Opačić, N. Lazarević, M. Šćepanović, H. Ryu, H. Lei, C. Petrović, and Z. V. Popović, Evidence of superconductivity-induced phonon spectra renormalization in alkali-doped iron selenides, *J. Phys.: Condens. Matter* **27**, 485701 (2015).
- [29] A. Baum, A. Milosavljević, N. Lazarević, M. M. Radonjić, B. Nikolić, M. Mitschek, Z. Inanloo Maranloo, M. Šćepanović, M. Grujić-Brojčin, N. Stojilović, M. Opel, Aifeng Wang, C. Petrović, Z. V. Popović, and R. Hackl, Phonon anomalies in FeS, *Phys. Rev. B* **97**, 054306 (2018).
- [30] N. Lazarević, M. Radonjić, M. Šćepanović, Hechang Lei, D. Tanasković, C. Petrović, and Z. V. Popović, Lattice dynamics of KNi<sub>2</sub>Se<sub>2</sub>, *Phys. Rev. B* **87**, 144305 (2013).

- [31] N. Lazarević, Z. V. Popović, Rongwei Hu, and C. Petrović, Evidence for electron-phonon interaction in  $\text{Fe}_{1-x}M_x\text{Sb}_2$  ( $M = \text{Co}$  and  $\text{Cr}$ ;  $0 \leq x \leq 0.5$ ) single crystals, *Phys. Rev. B* **81**, 144302 (2010).
- [32] L. J. Sandilands, Y. Tian, K. W. Plumb, Y.-J. Kim, and K. S. Burch, Scattering Continuum and Possible Fractionalized Excitations in  $\alpha$ -RuCl<sub>3</sub>, *Phys. Rev. Lett.* **114**, 147201 (2015).

## Lattice dynamics and phase transition in CrI<sub>3</sub> single crystals

S. Djurdjić-Mijin,<sup>1</sup> A. Šolajić,<sup>1</sup> J. Pešić,<sup>1</sup> M. Šćepanović,<sup>1</sup> Y. Liu (刘育),<sup>2</sup> A. Baum,<sup>3,4</sup> C. Petrović,<sup>2</sup> N. Lazarević,<sup>1</sup> and Z. V. Popović<sup>1,5</sup>

<sup>1</sup>Center for Solid State Physics and New Materials, Institute of Physics Belgrade, University of Belgrade, Pregrevica 118, 11080 Belgrade, Serbia

<sup>2</sup>Condensed Matter Physics and Materials Science Department, Brookhaven National Laboratory, Upton, New York 11973-5000, USA

<sup>3</sup>Walther Meissner Institut, Bayerische Akademie der Wissenschaften, 85748 Garching, Germany

<sup>4</sup>Fakultät für Physik E23, Technische Universität München, 85748 Garching, Germany

<sup>5</sup>Serbian Academy of Sciences and Arts, Knez Mihailova 35, 11000 Belgrade, Serbia



(Received 9 July 2018; published 18 September 2018)

The vibrational properties of CrI<sub>3</sub> single crystals were investigated using Raman spectroscopy and were analyzed with respect to the changes of the crystal structure. All but one mode are observed for both the low-temperature  $R\bar{3}$  and the high-temperature  $C2/m$  phase. For all observed modes the energies and symmetries are in good agreement with DFT calculations. The symmetry of a single layer was identified as  $p\bar{3}1/m$ . In contrast to previous studies we observe the transition from the  $R\bar{3}$  to the  $C2/m$  phase at 180 K and find no evidence for coexistence of both phases over a wide temperature range.

DOI: [10.1103/PhysRevB.98.104307](https://doi.org/10.1103/PhysRevB.98.104307)

### I. INTRODUCTION

Two-dimensional layered materials have gained attention due to their unique properties, the potential for a wide spectrum of applications, and the opportunity for the development of functional van der Waals heterostructures. CrI<sub>3</sub> is a member of the chromium-trihalide family which are ferromagnetic semiconductors [1]. Recently they have received significant attention as candidates for the study of magnetic monolayers. The experimental realization of CrI<sub>3</sub> ferromagnetic monolayers [1] motivated further efforts towards their understanding. CrI<sub>3</sub> features electric field controlled magnetism [2] as well as a strong magnetic anisotropy [3,4]. With the main absorption peaks lying in the visible part of the spectrum, it is a great candidate for low-dimensional semiconductor spintronics [5]. In its ground state, CrI<sub>3</sub> is a ferromagnetic semiconductor with a Curie temperature of 61 K [1,6] and a band gap of 1.2 eV [6]. It was demonstrated that the magnetic properties of CrI<sub>3</sub> mono- and bilayers can be controlled by electrostatic doping [2]. Upon cooling, CrI<sub>3</sub> undergoes a phase transition around 220 K from the high-temperature monoclinic ( $C2/m$ ) to the low-temperature rhombohedral ( $R\bar{3}$ ) phase [3,7]. Although the structural phase transition is reported to be first order, it was suggested that the phases may coexist over a wide temperature range [3]. Raman spectroscopy can be of use here due to its capability to simultaneously probe both phases in a phase-separated system [8–10].

A recent theoretical study predicted the energies of all Raman active modes in the low-temperature and high-temperature structure of CrI<sub>3</sub> suggesting a near degeneracy between the  $A_g$  and  $B_g$  modes in the monoclinic ( $C2/m$ ) structure. Their energies match the energies of  $E_g$  modes in the rhombohedral ( $R\bar{3}$ ) structure [7].

In this article we present an experimental and theoretical Raman scattering study of CrI<sub>3</sub> lattice dynamics. In both phases all but one of the respective modes predicted by

symmetry were observed. The energies for all modes are in good agreement with the theoretical predictions for the assumed crystal symmetry. Our data suggest that the first-order transition occurs at  $T_s \approx 180$  K without evidence for phase coexistence over a wide temperature range.

### II. EXPERIMENT AND NUMERICAL METHOD

The preparation of the single crystal CrI<sub>3</sub> sample used in this study is described elsewhere [11]. The Raman scattering experiment was performed using a Tri Vista 557 spectrometer in backscattering micro-Raman configuration with a 1800/1800/2400 grooves/mm diffraction grating combination. The 532 nm line of a Coherent Verdi G solid state laser was used for excitation. The direction of the incident light coincides with the crystallographic  $c$  axis. The sample was oriented so that its principal axis of the  $R\bar{3}$  phase coincides with the  $x$  axis of the laboratory system. A KONTI CryoVac continuous helium flow cryostat with a 0.5-mm-thick window was used for measurements at all temperatures under high vacuum ( $10^{-6}$  mbar). The sample was cleaved in air before being placed into the cryostat. The obtained Raman spectra were corrected by the Bose factor and analyzed quantitatively by fitting Voigt profiles to the data whereby the Gaussian width  $\Gamma_{\text{Gauss}} = 1 \text{ cm}^{-1}$  reflects the resolution of the spectrometer.

The spin polarized density functional theory (DFT) calculations have been performed in the Quantum Espresso (QE) software package [12] using the Perdew-Burke-Ernzerhof (PBE) exchange-correlation functional [13] and PAW pseudopotentials [14,15]. The energy cutoffs for the wave functions and the charge density were set to be 85 and 425 Ry, respectively, after convergence tests. For  $k$ -point sampling, the Monkhorst-Pack scheme was used with a  $8 \times 8 \times 8$  grid centered around the  $\Gamma$  point. Optimization of the atomic positions in the unit cell was performed until the interatomic forces

were smaller than  $10^{-6}$  Ry/Å. To treat the van der Waals (vdW) interactions a Grimme-D2 correction [16] is used in order to include long-ranged forces between the layers, which are not properly captured within LDA or GGA functionals. This way, the parameters are obtained more accurately, especially the interlayer distances. Phonon frequencies were calculated at the  $\Gamma$  point using the linear response method implemented in QE. The phonon energies are compiled in Table III together with the experimental values. The eigenvectors of the Raman active modes for both the low- and high-temperature phase are depicted in Fig. 5 of the Appendix.

### III. RESULTS AND DISCUSSION

$\text{CrI}_3$  adopts a rhombohedral  $R\bar{3}$  ( $C_{3i}^2$ ) crystal structure at low temperatures and a monoclinic  $C2/m$  ( $C_{2h}^3$ ) crystal structure at room temperature [3], as shown in Fig. 1. The main difference between the high- and low-temperature crystallographic space groups arises from different stacking sequences with the  $\text{CrI}_3$  layers being almost identical. In the rhombohedral structure the Cr atoms in one layer are placed above the center of a hole in the Cr honeycomb net of the two adjacent layers. When crossing the structural phase transition at  $T_s$  to the monoclinic structure the layers are displaced along the  $a$  direction so that every fourth layer is at the same place as the first one. The interatomic distances, mainly the interlayer distance, and the vdW gap, are slightly changed by the structural transition. The crystallographic parameters for both phases are presented in Table I. The numerically obtained values are in good agreement with reported x-ray diffraction data [11].

The vibrational properties of layered materials are typically dominated by the properties of the single layers composing the crystal. The symmetry of a single layer can be described by one of the 80 diperiodic space groups (DG) obtained by

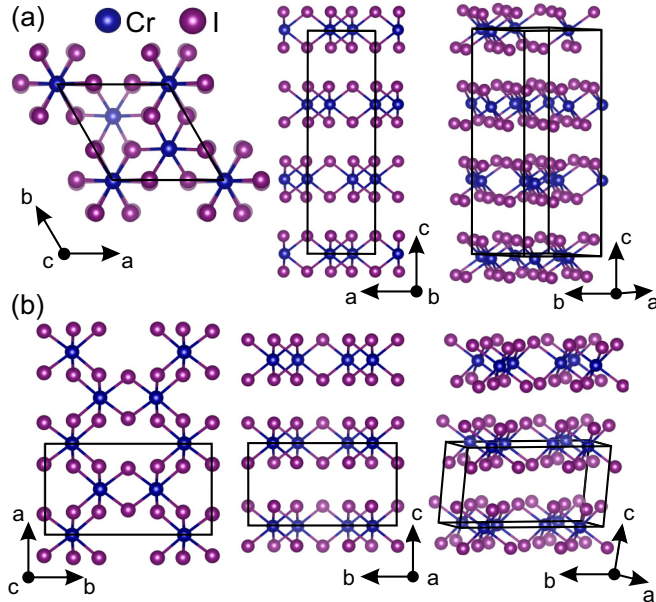


FIG. 1. Schematic representation of (a) the low-temperature  $R\bar{3}$  and (b) the high-temperature  $C2/m$  crystal structure of  $\text{CrI}_3$ . Black lines represent unit cells.

TABLE I. Calculated and experimental [11] parameters of the crystallographic unit cell for the low-temperature  $R\bar{3}$  and high-temperature  $C2/m$  phase of  $\text{CrI}_3$ .

$T$ (K)	Space group $R\bar{3}$		Space group $C2/m$	
	Calc.	Expt. [11]	Calc.	Expt. [11]
$a$ (Å)	6.87	6.85	6.866	6.6866
$b$ (Å)	6.87	6.85	11.886	11.856
$c$ (Å)	19.81	19.85	6.984	6.966
$\alpha$ (deg)	90	90	90	90
$\beta$ (deg)	90	90	108.51	108.68
$\gamma$ (deg)	120	120	90	90

lifting translational invariance in the direction perpendicular to the layer [17]. In the case of  $\text{CrI}_3$ , the symmetry analysis revealed that the single layer structure is fully captured by the  $p\bar{3}1/m$  ( $D_{3d}^1$ ) diperiodic space group DG71, rather than by  $R\bar{3}2/m$  as proposed in Ref. [7].

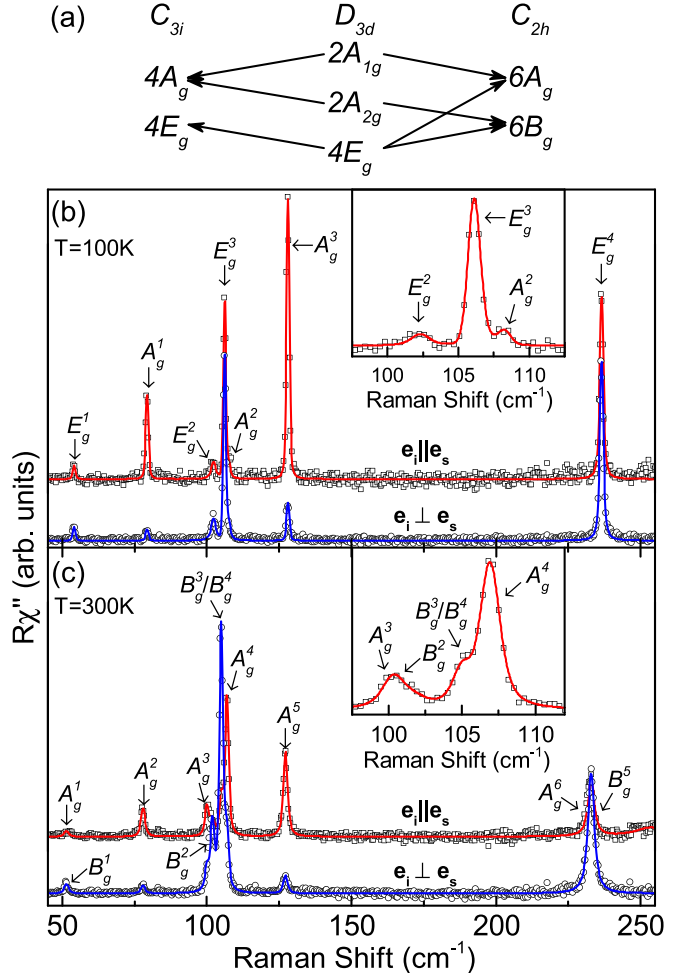


FIG. 2. (a) Compatibility relations for the  $\text{CrI}_3$  layer and the crystal symmetries. Raman spectra of (b) the low-temperature  $R\bar{3}$  and (c) the high-temperature  $C2/m$  crystal structure measured in parallel (open squares) and crossed (open circles) polarization configurations at 100 and 300 K, respectively. Red and blue solid lines represent fits of Voigt profiles to the experimental data.

TABLE II. Wyckoff positions of the two types of atoms and their contributions to the  $\Gamma$ -point phonons for the  $R\bar{3}$  and  $C2/m$  as well as the  $p\bar{3}1/m$  diperiodic space group. The second row shows the Raman tensors for the corresponding space groups.

Space group $R\bar{3}$		Diperiodic space group $p\bar{3}1/m$		Space group: $C2/m$	
Atoms	Irreducible representations	Atoms	Irreducible representations	Atoms	Irreducible representations
Cr (6c)	$A_g + A_u + E_g + E_u$	Cr (2c)	$A_{2g} + A_{2u} + E_g + E_u$	Cr (4g)	$A_g + A_u + 2B_g + 2B_u$
I (18f)	$3A_g + 3A_u + 3E_g + 3E_u$	I (6k)	$2A_{1g} + A_{1u} + A_{2g} + 2A_{2u} + 3E_g + 3E_u$	I (4i)	$2A_g + 2A_u + B_g + B_u$
				I (8j)	$3A_g + 3A_u + 3B_g + 3B_u$
	$A_g = \begin{pmatrix} a & & \\ & a & \\ & & b \end{pmatrix}$		$A_{1g} = \begin{pmatrix} a & & \\ & a & \\ & & b \end{pmatrix}$		$A_g = \begin{pmatrix} a & d \\ c & \\ d & b \end{pmatrix}$
	$^1E_g = \begin{pmatrix} c & d & e \\ d & -c & f \\ e & f & \end{pmatrix}$	$^2E_g = \begin{pmatrix} d & -c & -f \\ -c & -d & e \\ -f & e & \end{pmatrix}$	$^1E_g = \begin{pmatrix} c & & \\ & -c & d \\ & d & \end{pmatrix}$	$^2E_g = \begin{pmatrix} & -c & -d \\ -c & & \\ -d & e & \end{pmatrix}$	$B_g = \begin{pmatrix} e & \\ f & \end{pmatrix}$

According to the factor group analysis (FGA) for a single CrI<sub>3</sub> layer, six modes ( $2A_{1g} + 4E_g$ ) are expected to be observed in the Raman scattering experiment (see Table II). By stacking the layers the symmetry is reduced and, depending on the stacking sequence, FGA yields a total of eight Raman active modes ( $4A_g + 4E_g$ ) for the  $R\bar{3}$  and 12 Raman active modes ( $6A_g + 6B_g$ ) for the  $C2/m$  crystal symmetry. The correlation between layer and crystal symmetries for both cases is shown in Fig. 2(a) [18,19].

Figure 2(b) shows the CrI<sub>3</sub> single crystal Raman spectra measured at 100 K in two scattering channels. According to the selection rules for the rhombohedral crystal structure (Table II) the  $A_g$  modes can be observed only in the parallel polarization configuration, whereas the  $E_g$  modes appear in both parallel and crossed polarization configurations. Based on the selection rules the peaks at about 78, 108, and 128 cm<sup>-1</sup> were identified as  $A_g$  symmetry modes, whereas the peaks at about 54, 102, 106, and 235 cm<sup>-1</sup> are assigned as  $E_g$  symmetry. The weak observation of the most pronounced  $A_g$  modes in crossed polarizations [Fig. 2(b)] is attributed to

the leakage due to a slight sample misalignment and/or the presence of defects in the crystal. The energies of all observed modes are compiled in Table III together with the energies predicted by our calculations and by Ref. [7], and are found to be in good agreement for the  $E_g$  modes. The discrepancy is slightly larger for the low energy  $A_g$  modes. Our calculations in general agree with those from Ref. [7]. The  $A_g^4$  mode of the rhombohedral phase, predicted by calculation to appears at about 195 cm<sup>-1</sup>, was not observed in the experiment, most likely due to its low intensity.

When the symmetry is lowered in the high-temperature monoclinic  $C2/m$  phase [Fig. 2(c)] the  $E_g$  modes split into an  $A_g$  and a  $B_g$  mode each, whereas the rhombohedral  $A_g^2$  and  $A_g^4$  modes are predicted to switch to the monoclinic  $B_g$  symmetry. The correspondence of the phonon modes across the phase transition is indicated by the arrows in Table III. The selection rules for  $C2/m$  (see Table II) predict that  $A_g$  and  $B_g$  modes can be observed in both parallel and crossed polarization configurations. Additionally, the sample forms three types of domains which are rotated with respect to each other. We

TABLE III. Phonon symmetries and phonon energies for the low-temperature  $R\bar{3}$  and high-temperature  $C2/m$  phase of CrI<sub>3</sub>. The experimental values were determined at 100 and 300 K, respectively. All calculations were performed at zero temperature. Arrows indicate the correspondence of the phonon modes across the phase transition.

Space group $R\bar{3}$				Space group $C2/m$				
Symm.	Expt. (cm <sup>-1</sup> )	Calc. (cm <sup>-1</sup> )	Calc. (cm <sup>-1</sup> ) [7]	Symm.	Expt. (cm <sup>-1</sup> )	Calc. (cm <sup>-1</sup> )	Calc. [7] (cm <sup>-1</sup> )	
$E_g^1$	54.1	59.7	53	$\nearrow\searrow$	$B_g^1$	52.0	57.0	52
$A_g^1$	73.33	89.6	79	$\longrightarrow$	$A_g^1$	53.6	59.8	51
$E_g^2$	102.3	99.8	98	$\nearrow\searrow$	$A_g^2$	78.6	88.4	79
$E_g^3$	106.2	112.2	102	$\nearrow\searrow$	$A_g^3$	101.8	101.9	99
$A_g^2$	108.3	98.8	88	$\longrightarrow$	$B_g^2$	102.4	101.8	99
$A_g^3$	128.1	131.1	125	$\longrightarrow$	$B_g^3$	106.4 <sup>a</sup>	108.9	101
$A_g^4$	—	195.2	195	$\longrightarrow$	$A_g^4$	108.3	109.3	102
$E_g^4$	236.6	234.4	225	$\nearrow\searrow$	$B_g^4$	106.4 <sup>a</sup>	97.8	86
					$A_g^5$	128.2	131.7	125
					$B_g^5$	—	198.8	195
					$A_g^6$	234.6	220.1	224
					$B_g^6$	235.5	221.1	225

<sup>a</sup>Observed as two peak structure.

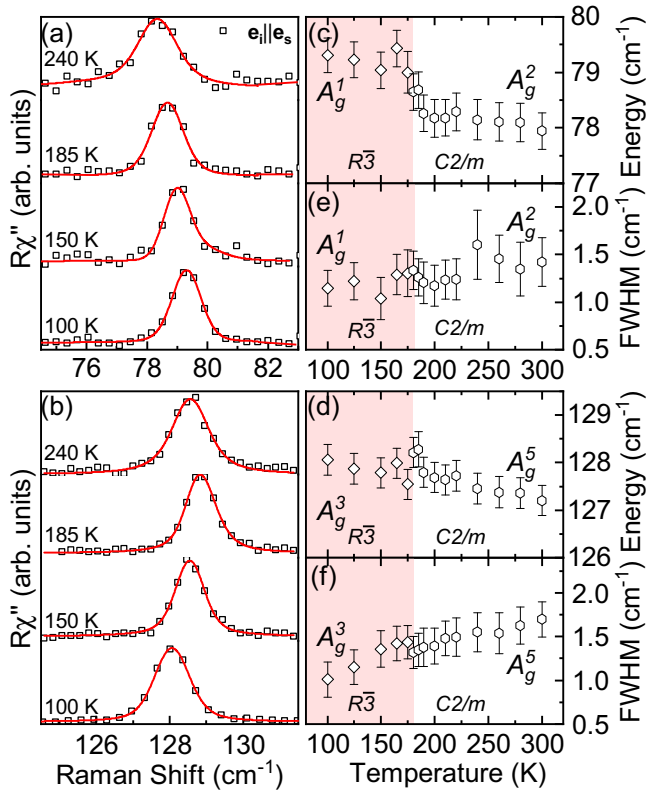


FIG. 3. Temperature dependence of the  $A_g^1$  and  $A_g^3$  phonon modes of the rhombohedral structure and the corresponding  $A_g^2$  and  $A_g^5$  modes of the monoclinic structure, respectively. (a) and (b) Raman spectra at temperatures as indicated. The spectra are shifted for clarity. Solid red lines represent Voigt profiles fitted to the data. (c) and (d) and (e) and (f) Temperature dependence of the phonon energies and linewidths, respectively. Both modes show an abrupt change in energy at the phase transition at 180 K.

therefore identify the phonons in the  $C2/m$  phase in relation to the calculations and find again good agreement of the energies. The  $B_g^3$  and  $B_g^4$  modes overlap and therefore cannot be resolved separately. As can be seen from the temperature dependence shown below [Fig. 4(b)] the peak at 106 cm<sup>-1</sup> broadens and gains spectral weight in the monoclinic phase in line with the expectation that two modes overlap. The missing rhombohedral  $A_g^4$  mode corresponds to the monoclinic  $B_g^5$  mode, which is likewise absent in the spectra.

The temperature dependence of the observed phonons is shown in Figs. 3 and 4. In the low-temperature rhombohedral phase all four  $E_g$  modes as well as  $A_g^1$  and  $A_g^2$  soften upon warming, whereas  $A_g^3$  hardens up to  $T \approx 180$  K before softening again. Crossing the first-order phase transition from  $R\bar{3}$  to  $C2/m$  crystal symmetry is reflected in the spectra as a symmetry change and/or renormalization for the non-degenerate modes and lifting of the degeneracy of the  $E_g$  modes as shown in Table II. In our samples, this transition is observed at  $T_s \approx 180$  K. The splitting of the  $E_g$  phonons into  $A_g$  and  $B_g$  modes at the phase transition is sharp (Fig. 4). The rhombohedral  $A_g^1$  and  $A_g^3$  phonons show a jump in energy and a small discontinuity in the linewidth at  $T_s$  (Fig. 3). Our spectra were taken during warming in multiple runs after

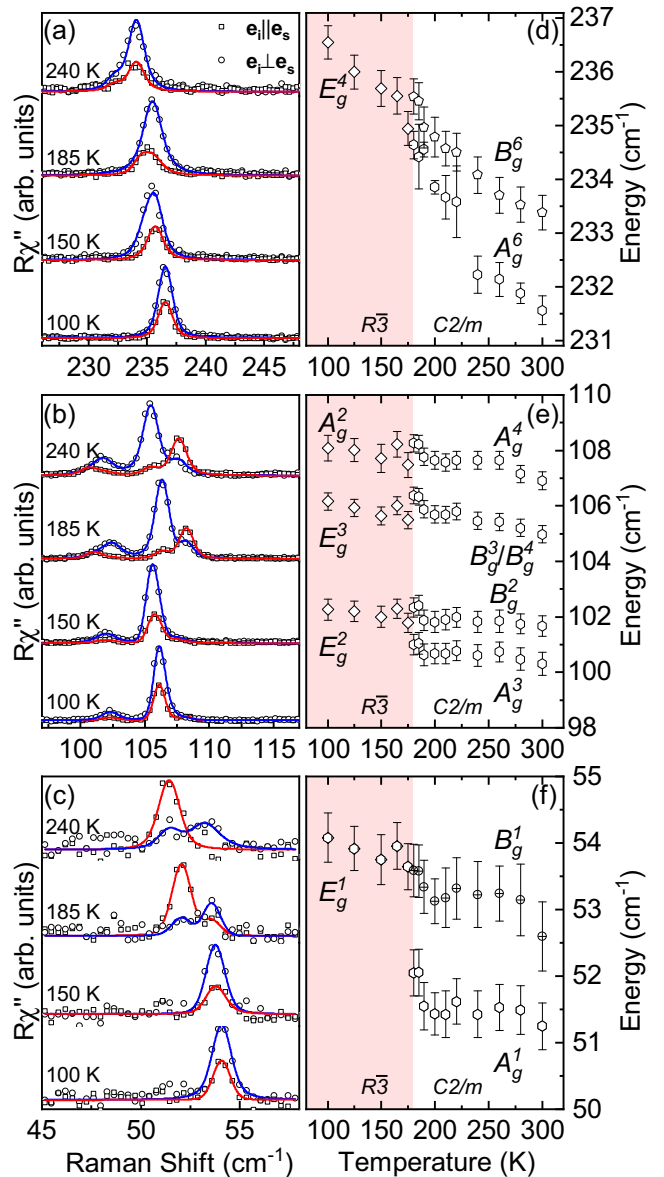


FIG. 4. Temperature dependence of the rhombohedral  $A_g^4$  and  $E_g$  modes. (a)–(c) Raman spectra in parallel (open squares) and crossed (open circles) light polarizations at temperatures as indicated. The spectra are shifted for clarity. Blue and red solid lines are fits of Voigt profiles to the data. Two spectra were analyzed simultaneously in two scattering channels with the integrated intensity as the only independent parameter. (d)–(f) Phonon energies obtained from the Voigt profiles. Each  $E_g$  mode splits into an  $A_g$  and a  $B_g$  mode above 180 K.

cooling to 100 K each time. We found that the temperature dependence for the phonon modes obtained this way was smooth in each phase. McGuire *et al.* [3,20] reported  $T_s$  in the range of 220 K, a coexistence of both phases and a large thermal hysteresis. However, they also noted that the first and second warming cycle showed identical behavior and only found a shift of the transition temperature to higher values for cooling cycles. We therefore consider the difference between the reported transition around 220 K and our  $T_s \approx 180$  K significant. To some extent this difference may be attributed

to local heating by the laser. More importantly, we find no signs of phase coexistence in the observed temperature range. The spectra for the low-temperature and high-temperature phases are distinctly different (Fig. 2) and the  $E_g$  modes exhibit a clearly resolved splitting which occurs abruptly at  $T_s$ . We performed measurements in small temperature steps (see Figs. 3 and 4). This limits the maximum temperature interval where the phase coexistence could occur in our samples to approximately 5 K, much less than the roughly 30 to 80 K reported earlier [3,20]. We cannot exclude the possibility that a small fraction of the low-temperature phase could still

coexist with the high-temperature phase over a wider temperature range, whereby weak peaks corresponding to the remains of the low-temperature  $R\bar{3}$  phase might be hidden under the strong peaks of the  $C2/m$  phase.

#### IV. CONCLUSION

We studied the lattice dynamics in single crystalline CrI<sub>3</sub> using Raman spectroscopy supported by numerical calculations. For both the low-temperature  $R\bar{3}$  and the high-temperature  $C2/m$  phase, all except one of the predicted

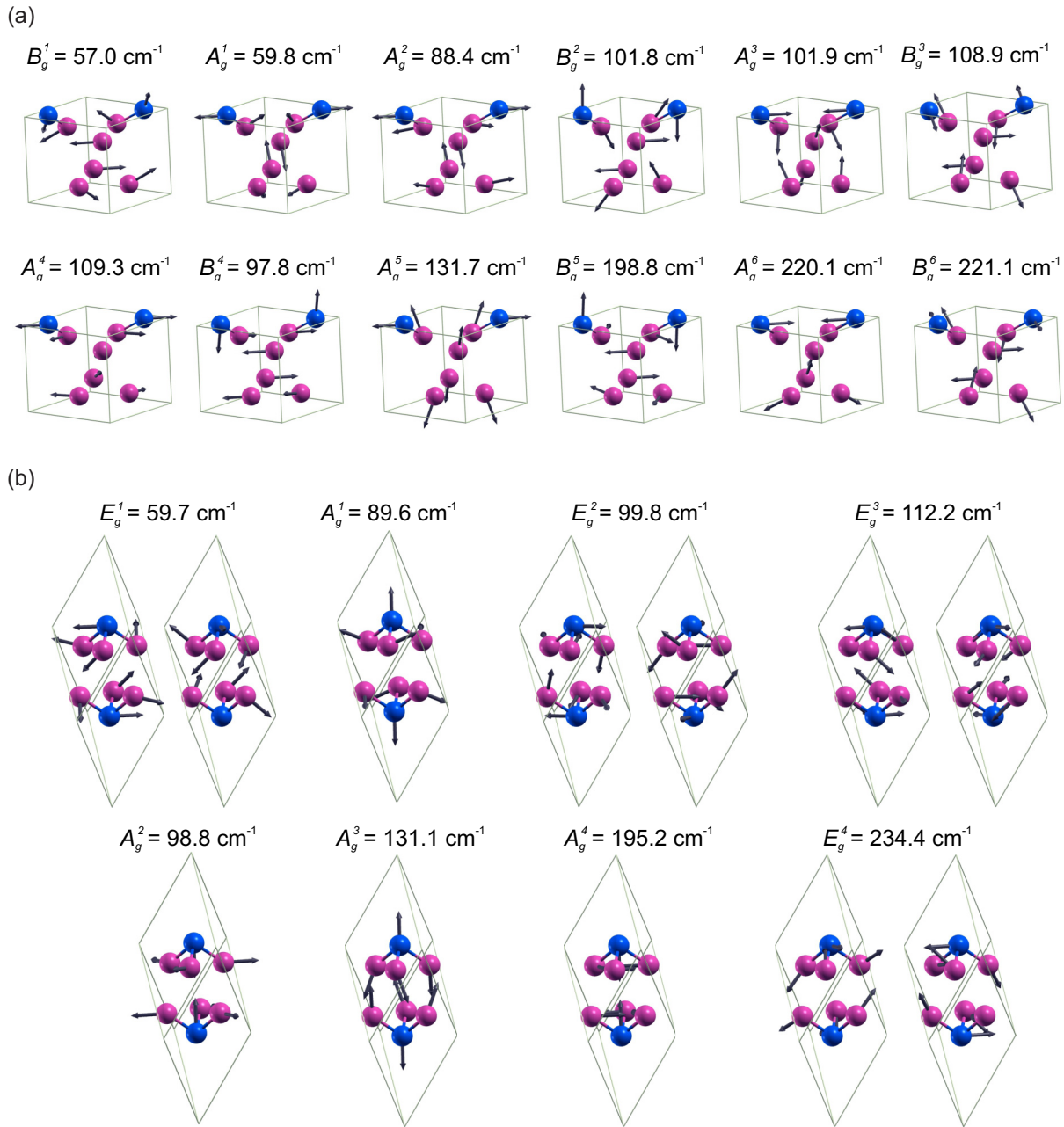


FIG. 5. Raman-active phonons in CrI<sub>3</sub> for (a) the monoclinic phase hosting  $A_g$  and  $B_g$  modes and for (b) the rhombohedral phase hosting  $A_g$  and  $E_g$  modes. Blue and violet spheres denote Cr and I atoms, respectively. Solid lines represent primitive unit cells. Arrow lengths are proportional to the square root of the interatomic forces. The given energies are calculated for zero temperature.

phonon modes were identified and the calculated and experimental phonon energies were found to be in good agreement. We determined that the symmetry of the single CrI<sub>3</sub> layers is  $p\bar{3}1/m$ . Abrupt changes to the spectra were found at the first-order phase transition which was located at  $T_s \approx 180$  K, lower than in previous studies. In contrast to the prior reports we found no sign of phase coexistence over temperature ranges exceeding 5 K.

## ACKNOWLEDGMENTS

The work was supported by the Serbian Ministry of Education, Science and Technological Development under Projects No. III45018 and No. OI171005. DFT calculations were performed using computational resources at Johannes Kepler University, Linz, Austria. Work at Brookhaven is supported by the U.S. DOE under Contract No. DE-SC0012704.

S.Dj.M. and N.L. conceived the experiment, performed the experiment, analyzed and discussed the data, and wrote the paper. A.Š. and J.P. calculated the phonon energies, analyzed and discussed the data, and wrote the paper. Y.L. and C.P. synthesized and characterized the samples. M.Š. performed the experiment and analyzed and discussed the data. A.B. and Z.V.P. analyzed and discussed the data and wrote the paper. All authors commented on the manuscript.

## APPENDIX: EIGENVECTORS

In addition to the phonon energies we also calculated the phonon eigenvectors which are shown in Fig. 5(a) for the high-temperature monoclinic phase and in Fig. 5(b) for the low-temperature rhombohedral phase. The energies, as given, are calculated for zero temperature. The relative displacement of the atoms is denoted by the length of the arrows.

- 
- [1] E. Navarro-Moratalla, B. Huang, G. Clark *et al.*, Layer-dependent ferromagnetism in a van der Waals crystal down to the monolayer limit, *Nature (London)* **546**, 270 (2017).
  - [2] S. Jiang, L. Li, Z. Wang, K. F. Mak, and J. Shan, Controlling magnetism in 2D CrI<sub>3</sub> by electrostatic doping, *Nat. Nanotechnol.* **13**, 549 (2018).
  - [3] M. A. McGuire, H. Dixit, V. R. Cooper, and B. C. Sales, Coupling of crystal structure and magnetism in the layered, ferromagnetic insulator CrI<sub>3</sub>, *Chem. Mater.* **27**, 612 (2015).
  - [4] J. L. Ladno and J. Fernández-Rossier, On the origin of magnetic anisotropy in two dimensional CrI<sub>3</sub>, *2D Mater.* **4**, 035002 (2017).
  - [5] W.-B. Zhang, Q. Qu, P. Zhu, and C.-H. Lam, Robust intrinsic ferromagnetism and half semiconductivity in stable two-dimensional single-layer chromium trihalides, *J. Mater. Chem. C* **3**, 12457 (2015).
  - [6] J. F. Dillon, Jr. and C. E. Olson, Magnetization, resonance, and optical properties of the ferromagnet CrI<sub>3</sub>, *J. Appl. Phys.* **36**, 1259 (1965).
  - [7] D. T. Larson and E. Kaxiras, Raman Spectrum of CrI<sub>3</sub>: An *ab initio* study, *Phys. Rev. B* **98**, 085406 (2018).
  - [8] N. Lazarević, M. Abeykoon, P. W. Stephens, H. Lei, E. S. Bozin, C. Petrovic, and Z. V. Popović, Vacancy-induced nanoscale phase separation in K<sub>x</sub>Fe<sub>2-y</sub>Se<sub>2</sub> single crystals evidenced by Raman scattering and powder x-ray diffraction, *Phys. Rev. B* **86**, 054503 (2012).
  - [9] H. Ryu, M. Abeykoon, K. Wang, H. Lei, N. Lazarević, J. B. Warren, E. S. Bozin, Z. V. Popovic, and C. Petrovic, Insulating and metallic spin glass in Ni-doped K<sub>x</sub>Fe<sub>2-y</sub>Se<sub>2</sub> single crystals, *Phys. Rev. B* **91**, 184503 (2015).
  - [10] H. Ryu, K. Wang, M. Opacic, N. Lazarevic, J. B. Warren, Z. V. Popovic, E. S. Bozin, and C. Petrovic, Sustained phase separation and spin glass in Co-doped K<sub>x</sub>Fe<sub>2-y</sub>Se<sub>2</sub> single crystals, *Phys. Rev. B* **92**, 174522 (2015).
  - [11] Y. Liu and C. Petrovic, Three-dimensional magnetic critical behavior in CrI<sub>3</sub>, *Phys. Rev. B* **97**, 014420 (2018).
  - [12] P. Giannozzi, S. Baroni, N. Bonini, M. Calandra, R. Car, C. Cavazzoni, D. Ceresoli, G. L. Chiarotti, M. Cococcioni, I. Dabo, A. D. Corso, S. de Gironcoli, S. Fabris, G. Fratesi, R. Gebauer, U. Gerstmann, C. Gougoussis, A. Kokalj, M. Lazzeri, L. Martin-Samos, N. Marzari, F. Mauri, R. Mazzarello, S. Paolini, A. Pasquarello, L. Paulatto, C. Sbraccia, S. Scandolo, G. Sclauzero, A. P. Seitsonen, A. Smogunov, P. Umari, and R. M. Wentzcovitch, Quantum espresso: A modular and open-source software project for quantum simulations of materials, *J. Phys. Condens. Matter* **21**, 395502 (2009).
  - [13] J. P. Perdew, K. Burke, and M. Ernzerhof, Generalized Gradient Approximation Made Simple, *Phys. Rev. Lett.* **77**, 3865 (1996).
  - [14] P. E. Blöchl, Projector augmented-wave method, *Phys. Rev. B* **50**, 17953 (1994).
  - [15] G. Kresse and D. Joubert, From ultrasoft pseudopotentials to the projector augmented-wave method, *Phys. Rev. B* **59**, 1758 (1999).
  - [16] S. Grimme, Semiempirical GGA-type density functional constructed with a long-range dispersion correction, *J. Comput. Chem.* **27**, 1787 (2006).
  - [17] E. A. Wood, The 80 diperiodic groups in three dimensions, *Bell Syst. Tech. J.* **43**, 541 (1964).
  - [18] W. G. Fateley, N. T. McDevitt, and F. F. Bentley, Infrared and raman selection rules for lattice vibrations: The correlation method, *Appl. Spectrosc.* **25**, 155 (1971).
  - [19] N. Lazarević, Z. V. Popović, R. Hu, and C. Petrovic, Evidence of coupling between phonons and charge-density waves in ErTe<sub>3</sub>, *Phys. Rev. B* **83**, 024302 (2011).
  - [20] M. A. McGuire, G. Clark, S. KC, W. M. Chance, G. E. Jellison, V. R. Cooper, X. Xu, and B. C. Sales, Magnetic behavior and spin-lattice coupling in cleavable van der Waals layered CrCl<sub>3</sub> crystals, *Phys. Rev. Mater.* **1**, 014001 (2017).



# Ab-initio calculations of electronic and vibrational properties of Sr and Yb intercalated graphene

Andrijana Šolajić<sup>1</sup> · Jelena Pešić<sup>1</sup> · Radoš Gajic<sup>1</sup>

Received: 14 October 2017 / Accepted: 14 June 2018  
© Springer Science+Business Media, LLC, part of Springer Nature 2018

## Abstract

Since the 1960s, Graphite intercalation compounds (GIC) have been extensively studied, showing many new properties and exotic physics. This inspired many to investigate a single or few-layer intercalated graphene. Intercalated graphene has many extraordinary properties and it is different compared to pristine graphene or bulk GICs, with great spectra of characteristics induced by various intercalants. This method opens new possibilities for research and applications in electronics and photonics. Here we present the results of a DFT study on electronic and vibrational properties of the graphene doped with Sr and Yb adatoms, taking into account that only their corresponding bulk compounds have been investigated so far. The calculations were performed in Quantum Espresso software package.

**Keywords** Graphene · DFT · Electronic properties · 2D materials

## 1 Introduction

Since the experimental discovery in Novoselov et al. (2004), graphene has been attracting enormous attention. The relativistic behaviour of the low-energy excitations (the so-called *Dirac fermions*) leads to many interesting effects and the linear electronic dispersion of graphene in the vicinity of the K-point mimics the physics of the massless fermions in quantum electrodynamics, at speed 300 times smaller than the speed of light. Therefore, many unusual properties can be observed in graphene, such are the Klein paradox (Katsnelson et al. 2006) or the anomalous integer quantum Hall effect (Gusynin and Sharapov 2005; Neto et al. 2006) which can be observed at room temperatures (Novoselov et al. 2007).

---

This article is part of the Topical Collection on Focus on Optics and Bio-photonics, Photonica 2017.

---

Guest Edited by Jelena Radovanovic, Aleksandar Krmpot, Marina Lekic, Trevor Benson, Mauro Pereira, Marian Marciniak.

---

✉ Andrijana Šolajić  
solajic@ipb.ac.rs

<sup>1</sup> Laboratory for Graphene, Other 2D Materials and Ordered Nanostructures, Center for Solid State Physics and New Materials, Institute of Physics Belgrade, University of Belgrade, Pregrevica 118, Belgrade 11080, Serbia

Graphene has excellent thermal conductivity, high electron mobility (Bolotin et al. 2008) and transparency, and at the same time it is one of the strongest materials known (Lee et al. 2008), about 200 times stronger than structural steel, yet very flexible and stretchable. With all its unique properties, graphene has various potential applications in almost all research fields, especially in electronics and optoelectronics (Ferrari 2015; Blake et al. 2008; Todorović et al. 2015). With high electrical and optical conductivity, it is promising candidate for applications in energy storage (Bonaccorso et al. 2015), detectors (Sassi et al. 2017; Liu et al. 2014), or even for the flexible touch screen technology (Ahn and Hong 2014; Bae et al. 2010). Ultra-thin graphitic films are also well researched for applications in photonics with high transparency and electrical conductivity (Matković et al. 2016).

Already extraordinary characteristics of graphene can be tailored and enhanced in many ways—by various types of disorders, controlling the type of edges (Peres et al. 2006; Wakabayashi et al. 1996, 2009), number of layers, by doping, applying the strain (Levy et al. 2010; Choi et al. 2010; Settnes et al. 2016; Masir et al. 2013), etc. Among them, doping graphene is an excellent way to make graphene suitable for various applications (Sharma and Ahn 2013; Wang et al. 2010; Qu et al. 2010; Jeong et al. 2011; Cui et al. 2011). Especially interesting is intercalation of various species in a few layer graphene (or doping a single layer graphene with adatoms), in a similar manner to the graphite intercalation compounds (GIC). This provides very high level of doping and leads to many interesting effects that are not present in pristine graphene, offering a new way to design various materials with magnetic, highly conductive or superconducting properties. Doping via adsorption is also very convenient, as the graphene can host various adatoms or small molecules while preserving its own structure, and at the same time drastically change its electronic properties. By covering the graphene sheet with the layer of adatoms, significant structural changes are avoided, as the dopant atoms are not fitted in the graphene lattice instead of the carbon atoms. However, adsorbed atoms can strongly affect the electronic properties of graphene, dominantly through the  $p_z$  orbitals. Therefore, it is an excellent tool for tuning the properties of graphene in a wide range and obtain new effects. GIC have been extensively researched since the 1960s (Rüdorff 1959; Enoki et al. 2003; Dresselhaus and Dresselhaus 2002), but the interest for them has significantly raised with discovery of the superconductivity in some of the alkali or alkaline earth metal intercalated graphite structures, among which are  $\text{CaC}_6$  and  $\text{YbC}_6$  (Weller et al. 2005) with relatively high critical temperatures of  $T_c = 11.5\text{ K}$  and  $T_c = 6.5\text{ K}$ . As research of 2D materials has raised in the last decade, the superconductivity in GIC imposed a question of investigating the monolayer graphene doped with alkali and alkaline earth metal adatoms, searching for the atomically thin superconductors. The electrical characteristics of the doped graphene depend strongly on the species of the used adatom. Reports on related structures suggest the occurrence of superconductivity in some of them, usually with alkali or alkaline earth metals doping, similar to the GICs. The explanation for the emergence of the superconductivity in the alkali doped graphene lies in the electron-phonon coupling that arises from the new intercalant-derived band and the graphene  $\pi$ -bands at the Fermi level. Among first researched doped graphene structures was Li decorated graphene (Profeta et al. 2012; Pešić et al. 2015), which is superconducting with the critical temperature of  $T = 5.9\text{ K}$ . It can also be enhanced by applying the strain (Pešić et al. 2014). The experimental evidence of superconductivity in the Li doped graphene (Ludbrook 2015) inspired many to search for other 2D superconducting structures (Calandra et al. 2012; Penev et al. 2016; Shimada et al. 2017; Saito et al. 2016). Graphene doped with the Ca atoms is also reported to be superconducting as the doped monolayer (Profeta et al. 2012) and bilayer intercalated graphene (Mazin and Balatsky 2010; Margine et al. 2016), there are also reports for a

few-layer potassium doped graphene (Xue et al. 2012). Among other similar structures, the heavily n-doped graphene was also predicted to be superconducting (Margine and Giustino 2014), the combination of biaxial strain with charge doping, which leads to the superconductor with  $T_c$  estimated to be up to 30 K (Si et al. 2013), or the hole-doped graphane which was predicted to be a high  $T_c$  superconductor, with a critical temperature in range 60–80 K (Durajski 2015). However, many possible structures based on doped graphene with potential superconducting properties are not considered yet.

In this paper we studied the electronic and vibrational properties of Sr and Yb doped graphene using the density functional theory approach. We were motivated by the fact that both structures are known as superconductors in their corresponding bulk compounds,  $\text{YbC}_6$  with critical temperature of  $T_c = 6.5$  K (Weller et al. 2005) and  $\text{SrC}_6$  with up to  $T_c = 3.03$  K (Calandra and Mauri 2006). We are first to report the results for a monolayer graphene doped with those adatoms.

## 2 Computational details

All calculations were performed using the Quantum Espresso software package (Giannozzi et al. 2009), based on the plane waves and pseudopotentials. We used norm-conserving pseudopotentials (Perdew and Zunger 1981) and LDA exchange-correlation functional. The plane wave energy cutoff is 120 Ry for  $\text{SrC}_6$ -mono and 160 Ry for  $\text{YbC}_6$ -mono. The unit cell for both structures is modelled as  $\sqrt{3} \times \sqrt{3}R30^\circ$  supercell of the graphene unit cell, with adatoms positioned in the H-site. This is the favorable adsorption site for both adatoms, according to the DFT study (Nakada and Ishii 2011). The value of the hexagonal cell parameter  $a$  is 4.26 Å taken theoretically, as there are no experimental realization of those structures. The top and side view of the structures are shown in Fig. 1. In order to avoid interactions between layers, the hexagonal cell parameter  $c$  of the unit cell was chosen to be sufficiently large,  $c = 11.4$  Å for  $\text{SrC}_6$ -mono and 11.3 Å for  $\text{YbC}_6$ -mono. Prior to any calculations, the ionic positions in systems are fully relaxed to their minimum energy configuration, using the Broyden-Fletcher-Goldfarb-Shanno (BFGS) algorithm. Obtained vertical distance between graphene layer and the adsorbed atom is  $h = 2.22$  Å for  $\text{SrC}_6$ -mono and  $h = 2.25$  Å for  $\text{YbC}_6$ -mono. Phonon properties are obtained with the Density

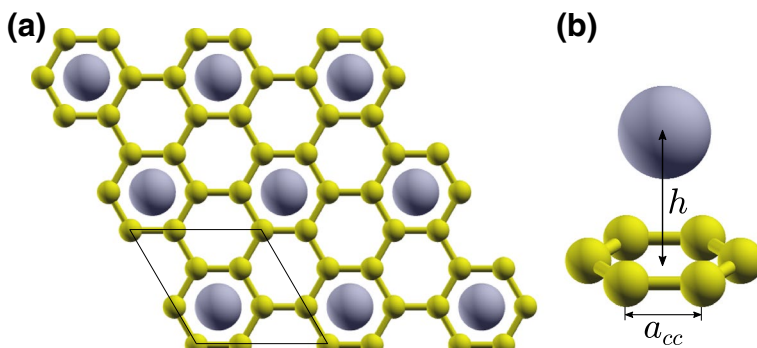


**Fig. 1** **a** Top view of the graphene structure with the adatoms adsorbed in the H-site. Unit cell is marked with the black line, **b** side view of the one hexagon with the adatom above

Functional Perturbation Theory (DFPT) implemented in the PHonon part of the Quantum Espresso software.

### 3 Results and discussion

As we said in Sect. 2, the unit cell for our H-site doped structures is enlarged compared to the pristine graphene. Due to the increase in the size of the primitive cell in direct space, basis vector lengths in reciprocal space are reduced. As a consequence, the K-point of the Brillouin zone of graphene is folded to the  $\Gamma$  point of the Brillouin zone of H-site doped graphene. Brillouin zones of the graphene unit cell and the H-site doped graphene are shown in Fig. 2.

#### 3.1 Electronic properties

Electronic dispersions along  $\Gamma$ -M-K- $\Gamma$  high symmetry points for SrC<sub>6</sub>-mono and YbC<sub>6</sub>-mono are shown in Fig. 3. Fermi level is set to zero in all figures. Folding the  $\pi$  and  $\pi^*$  bands of graphene from K-point to  $\Gamma$ -point, the inner and outer carbon  $\pi$  and  $\pi^*$  bands are obtained, crossing at the  $\Gamma$  point. For both structures, lower bands from the  $\sigma$  bonds in the valence band are almost unaffected, as expected, and they are not shown in figures. The Fermi level is shifted up in both structures. By deposition of adatoms on top of graphene, new interlayer band derived from the Yb or Sr adatoms is formed around the Fermi level, showing a nearly free-electron-like dispersion. They are placed at 2.2 and 1.5 eV below the Fermi level in the YbC<sub>6</sub>-mono and SrC<sub>6</sub>-mono, respectively, being partially occupied. The density of states on Fermi level is also raised. The carbon  $\pi$  bands are not affected by the presence of the adatoms. Previously unoccupied  $\pi^*$  bands now intersect the new up-shifted Fermi level and are strongly hybridized with the new band derived from the adsorbed atoms. In YbC<sub>6</sub>-mono, 4f orbitals coming from the Yb atoms form a set of flat non-dispersive bands, similar to the bulk YbC<sub>6</sub> (Csányi et al. 2005). Those flat bands are characteristic for most lanthanides. They are localized at 0.7 eV below the Fermi level with the corresponding peak clearly observed in the density of states. As reported for the bulk YbC<sub>6</sub>, calculations with the Hubbard+U corrections do not give significant changes and result only in slightly shifting down those bands, so the same is expected for the monolayer. The Dirac points from graphene are folded to the  $\Gamma$  point in the H-site doped graphene, and

**Fig. 2** Brillouin zones of graphene (black) and the H-site doped graphene (red). (Color figure online)

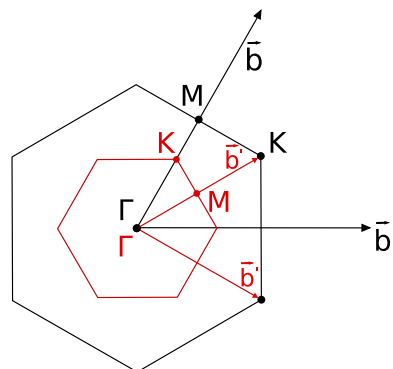
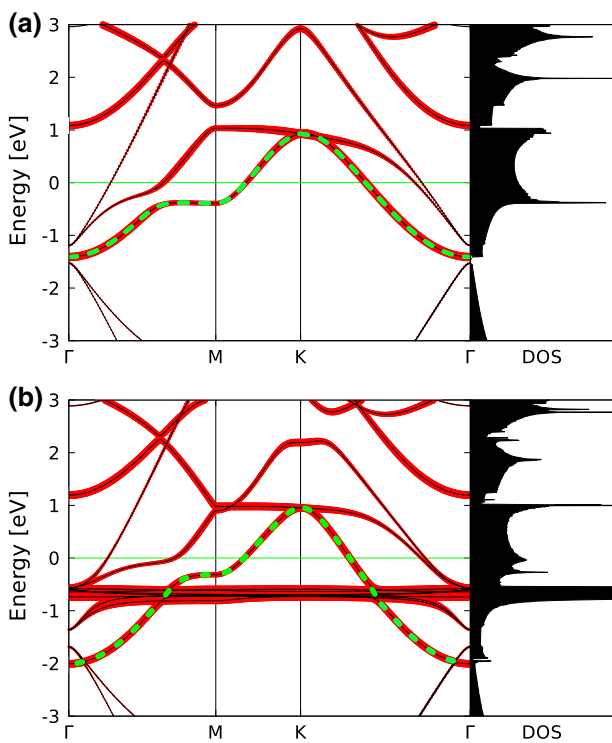


**Fig. 3** Electronic dispersions of a SrC<sub>6</sub>-mono and b YbC<sub>6</sub>-mono. Thickness of the red lines is proportional to the the Sr/Yb character and the interlayer band is marked in green dotted line. (Color figure online)



they are now below the Fermi level. Due to the adatom presence, the symmetry is broken and a gap is opened. In the SrC<sub>6</sub>, interlayer band is placed between the  $\pi$  and  $\pi^*$  and a very small gap can be observed in the density of states, while in the YbC<sub>6</sub>-mono, the new interlayer band intersect the  $\pi$  band and the gap is closed.

### 3.2 Phonon properties

The symmetry group of graphene with adatoms adsorbed in the H-site is  $Dg77 = T' C_{6v}$ , which is a subgroup of the diperiodic group of graphene,  $Dg80 = TD_{6h}$  (Damljanović et al. 2014). In order to connect the phonon modes of the H-site doped graphene with the corresponding phonon modes of graphene, the corresponding irreducible representation of group  $Dg77$  of graphene to its subgroup  $Dg80$  (Damljanović et al. 2014). The modes from the  $\Gamma$  point,  $\Gamma E_{2g}$  and  $\Gamma B_{1g}$  correspond to  $\Gamma E_2$  and  $\Gamma B_1$ . For the modes of graphene in the K point,  $KA'_1$  corresponds to the modes  $A_1$  and  $B_2$ ,  $KA'_2$  to  $A_2$  and  $B_1$ ,  $KE'$  and  $KE''$  to  $E_1$  and  $E_2$  (Altmann and Herzog 1994; Damljanović and Gajić 2012). The modes  $A_1$  and  $E_1$  are both infrared and Raman active, while  $E_2$  modes are only Raman active. The symmetry classification of optical modes and Raman tensors for H-site doped graphene are given in Table 1. The displacement patterns of the SrC<sub>6</sub>-mono and YbC<sub>6</sub>-mono, in the  $\Gamma$  point are shown in Fig. 4. Those modes have displacement patterns similar to those of graphene phonons at  $\Gamma$  and K points, which happens due to the Brillouin zone folding. As the K point of graphene is folded to the  $\Gamma$  point of the new Brillouin zone in the H-site doped graphene, the phonon modes in graphene at the  $\Gamma$  and K points correspond to the  $\Gamma$  modes in the H-site doped

**Table 1** Raman tensors and symmetry classification of optical modes

Raman tensors			
Graphene	$A_{1g}$	$E_{1g}$	$E_{2g}$
$Dg80 = TD_{6h}$	$\begin{pmatrix} a & 0 & 0 \\ 0 & a & 0 \\ 0 & 0 & b \end{pmatrix}$	$\begin{pmatrix} 0 & 0 & 0 \\ 0 & 0 & c \\ 0 & c & 0 \end{pmatrix}$	$\begin{pmatrix} d & 0 & 0 \\ 0 & -d & 0 \\ 0 & 0 & 0 \end{pmatrix}$
$O_z \parallel C_6$		$\begin{pmatrix} 0 & 0 & -c \\ 0 & 0 & 0 \\ c & 0 & 0 \end{pmatrix}$	$\begin{pmatrix} 0 & -d & 0 \\ -d & 0 & 0 \\ 0 & 0 & 0 \end{pmatrix}$
$O_x \parallel C'_2$			
$A\alpha$	$A_1$	$E_1$	$E_2$
$Dg77 = TC_{6v}$	$\begin{pmatrix} a & 0 & 0 \\ 0 & a & 0 \\ 0 & 0 & b \end{pmatrix}$	$\begin{pmatrix} 0 & 0 & c \\ 0 & 0 & 0 \\ c & 0 & 0 \end{pmatrix}$	$\begin{pmatrix} d & 0 & 0 \\ 0 & -d & 0 \\ 0 & 0 & 0 \end{pmatrix}$
$O_z \parallel C_6$		$\begin{pmatrix} 0 & 0 & 0 \\ 0 & 0 & c \\ 0 & c & 0 \end{pmatrix}$	$\begin{pmatrix} 0 & -d & 0 \\ -d & 0 & 0 \\ 0 & 0 & 0 \end{pmatrix}$
$O_x \parallel \sigma_v$			
Optical modes			
$A\alpha$		$\Gamma_{\text{opt}} = 2A_1 + A_2 + 2B_1 + B_2 + 3E_1 + 3E_2$	

structures. This is valid for all H-site doped graphene structures as the unit cell is the type. As the Kohn anomaly is present in graphene at  $\Gamma$  and K points in  $E_{2g}$  and  $KA'_1$  modes, we expect it to be present in the H-site doped graphene structures for the modes related to these two. Modes with Kohn anomaly can not be calculated precisely using the density functional theory as the DFT is based on the adiabatic Born-Oppenheimer approximation which is in this case broken. Comparing the calculated phonon modes for graphene at K and  $\Gamma$  point, with the corresponding phonon modes at the  $\Gamma$  point of the  $\text{SrC}_6$  and  $\text{YbC}_6$  monolayers, we can observe small differences in the corresponding frequencies. Some of these are lower than in pristine graphene and some frequencies are split. For example, frequencies of  $E_2$  mode in Sr and Yb doped graphene are  $1470\text{ cm}^{-1}$  and  $1488\text{ cm}^{-1}$ , respectively, while the frequency of  $E_{2g}$  in pristine graphene is  $1550\text{ cm}^{-1}$ ; Frequency of  $E'$  mode in graphene is  $1200\text{ cm}^{-1}$ , and corresponding modes in doped graphene are  $E_2$  at  $1180\text{ cm}^{-1}$  and  $E_1$  at  $1200\text{ cm}^{-1}$ ;  $E''$  mode in graphene is at  $580\text{ cm}^{-1}$ , and corresponding modes in doped graphene are  $E_2$  at  $495\text{ cm}^{-1}$  and  $E_1$  at  $510\text{ cm}^{-1}$  for  $\text{SrC}_6$ -mono and  $E_2$  at  $477\text{ cm}^{-1}$  and  $E_1$  at  $500\text{ cm}^{-1}$  for  $\text{YbC}_6$ -mono. This can be ascribed to the adatoms impact, and in general, it depends on the type of the adatom.

## 4 Conclusion

Using the density functional theory approach, we calculated the electronic and phonon properties of the Sr and Yb doped graphene, in a similar manner to the GICs. Their corresponding bulk compounds have been studied so far and we are first to investigate the monolayer graphene doped with those adatoms. The electronic and phonon properties are of essential interest for electron-phonon coupling as well as the guidelines for experimental research. From the electronic band structure calculations, we can observe a new adatom-derived interlayer band crossing the Fermi level in both structures, which hybridize strongly with the carbon  $p_z$  orbitals. Density of states on the Fermi level is also raised. Those results can be indicating a possible superconductivity and can be inspiring for further research of those structures. Displacement patterns calculated in the  $\Gamma$  point are similar to those in the K and  $\Gamma$  point of the pristine graphene, as a consequence of the zone folding effect, but due to the adatoms impact we can observe some differences in frequencies and the splitting of

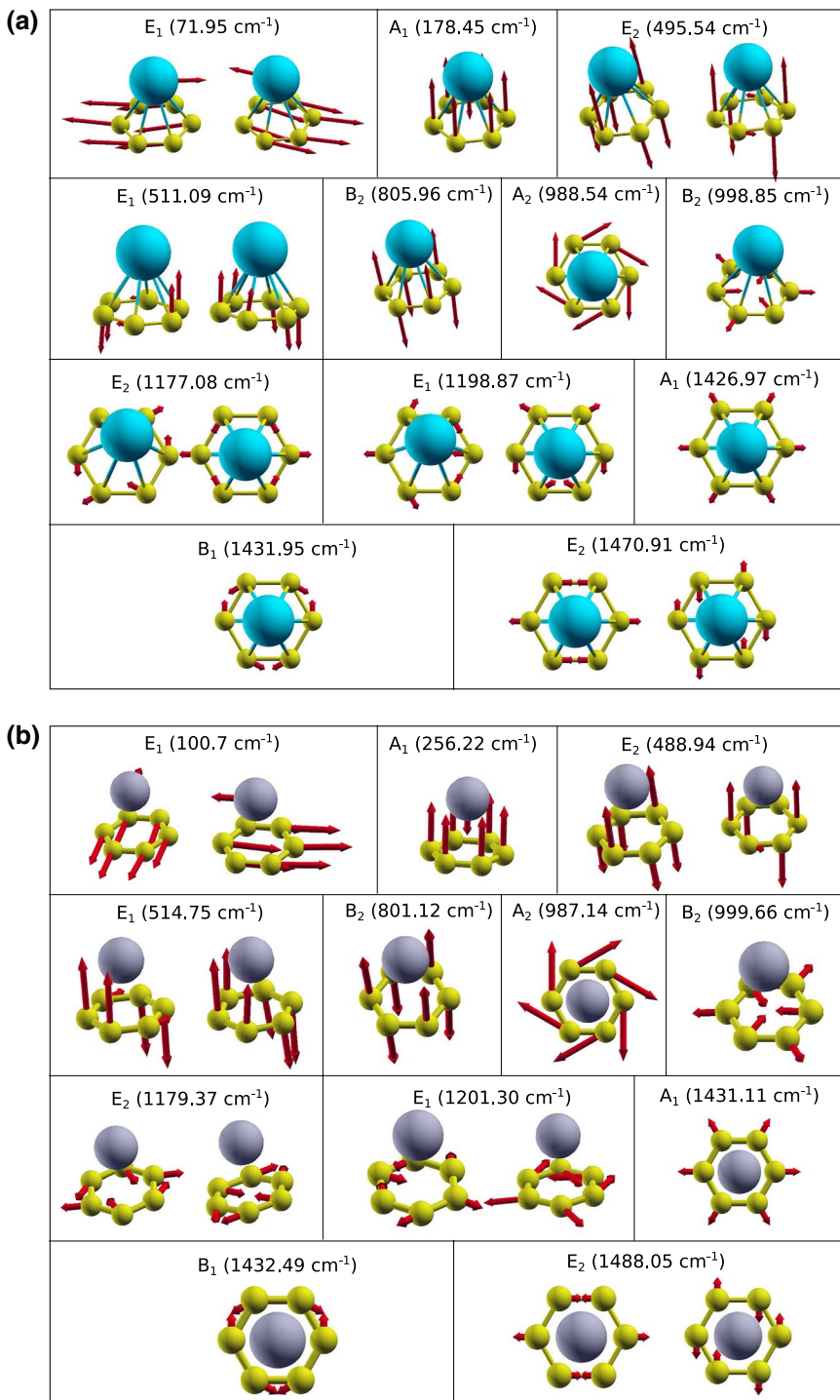


**Fig. 4** Displacement patterns of **a** SrC<sub>6</sub>-mono and **b** YbC<sub>6</sub>-mono. Acoustic modes ( $\omega = 0$ ) are not shown in pictures

some modes. The results obtained in this paper are important base for further theoretical and experimental research of those two structures, as well for future research of similar structures of graphene doped with other metal adatoms.

**Acknowledgements** This work is supported by the Serbian MPNTR through Project OI 171005 and by Qatar National Research Foundation through Project NPRP 7-665-1-12.

## References

- Ahn, J.H., Hong, B.H.: Graphene for displays that bend. *Nat. Nanotechnol.* **9**(10), 737–738 (2014)
- Altmann, S., Herzig, P.: Point-Group Theory Tables. Oxford Science Publications, Clarendon Press, Oxford (1994)
- Bae, S., Kim, H., Lee, Y., Xu, X., Park, J.S., Zheng, Y., Balakrishnan, J., Lei, T., Kim, H.R., Song, Y.I., et al.: Roll-to-roll production of 30-inch graphene films for transparent electrodes. *Nat. Nanotechnol.* **5**(8), 574–578 (2010)
- Blake, P., Brimicombe, P.D., Nair, R.R., Booth, T.J., Jiang, D., Schedin, F., Ponomarenko, L.A., Morozov, S.V., Gleeson, H.F., Hill, E.W., Geim, A.K., Novoselov, K.S.: Graphene-based liquid crystal device. *Nano Lett.* **8**(6), 1704–1708 (2008)
- Bolotin, K., Sikes, K., Jiang, Z., Klima, M., Fudenberg, G., Hone, J., Kim, P., Stormer, H.: Ultrahigh electron mobility in suspended graphene. *Solid State Commun.* **146**(9), 351–355 (2008)
- Bonaccorso, F., Colombo, L., Yu, G., Stoller, M., Tozzini, V., Ferrari, A.C., Ruoff, R.S., Pellegrini, V.: Graphene, related two-dimensional crystals, and hybrid systems for energy conversion and storage. *Science* **347**(6217), 1246501 (2015)
- Calandra, M., Mauri, F.: Possibility of superconductivity in graphite intercalated with alkaline earths investigated with density functional theory. *Phys. Rev. B* **74**, 094507 (2006)
- Calandra, M., Profeta, G., Mauri, F.: Superconductivity in metal-coated graphene. *Physica Status Solidi (B)* **249**(12), 2544–2548 (2012)
- Choi, S.M., Jhi, S.H., Son, Y.W.: Effects of strain on electronic properties of graphene. *Phys. Rev. B* **81**, 081407 (2010)
- Csányi, G., Littlewood, P., Nevidomskyy, A.H., Pickard, C.J., Simons, B.: The role of the interlayer state in the electronic structure of superconducting graphite intercalated compounds. *Nat. Phys.* **1**(1), 42–45 (2005)
- Cui, T., Lv, R., Huang, Z.H., Zhu, H., Zhang, J., Li, Z., Jia, Y., Kang, F., Wang, K., Wu, D.: Synthesis of nitrogen-doped carbon thin films and their applications in solar cells. *Carbon* **49**(15), 5022–5028 (2011)
- Damljanović, V., Kostić, R., Gajić, R.: Characters of graphenes symmetry group dg80. *Physica Scr.* **2014**(T162), 014022 (2014)
- Damljanović, V., Gajić, R.: Phonon eigenvectors of graphene at high-symmetry points of the Brillouin zone. *Physica Scr.* **2012**(T149), 014067 (2012)
- Dresselhaus, M.S., Dresselhaus, G.: Intercalation compounds of graphite. *Adv. Phys.* **51**(1), 1–186 (2002)
- Durajski, A.P.: Influence of hole doping on the superconducting state in graphane. *Supercond. Sci. Technol.* **28**(3), 035002 (2015)
- Enoki, T., Suzuki, M., Endo, M.: Graphite Intercalation Compounds and Applications, pp. 1–456. Oxford University Press, Oxford (2003)
- Ferrari, A.C., et al.: Science and technology roadmap for graphene, related two-dimensional crystals, and hybrid systems. *Nanoscale* **7**, 4598–4810 (2015)
- Giannozzi, P., et al.: Quantum espresso: a modular and open-source software project for quantum simulations of materials. *J. Phys. Condens. Matter* **21**(39), 395–502 (2009)
- Gusynin, V.P., Sharapov, S.G.: Unconventional integer quantum hall effect in graphene. *Phys. Rev. Lett.* **95**, 146801 (2005)
- Jeong, H.M., Lee, J.W., Shin, W.H., Choi, Y.J., Shin, H.J., Kang, J.K., Choi, J.W.: Nitrogen-doped graphene for high-performance ultracapacitors and the importance of nitrogen-doped sites at basal planes. *Nano Lett.* **11**(6), 2472–2477 (2011)
- Katsnelson, M., Novoselov, K., Geim, A.: Chiral tunnelling and the Klein paradox in graphene. *Nat. Phys.* **2**(9), 620–625 (2006)

- Lee, C., Wei, X., Kysar, J.W., Hone, J.: Measurement of the elastic properties and intrinsic strength of monolayer graphene. *Science* **321**(5887), 385–388 (2008)
- Levy, N., Burke, S.A., Meaker, K.L., Panlasigui, M., Zettl, A., Guinea, F., Neto, A.H.C., Crommie, M.F.: Strain-induced pseudo-magnetic fields greater than 300 tesla in graphene nanobubbles. *Science* **329**(5991), 544–547 (2010)
- Liu, C.H., Chang, Y.C., Norris, T.B., Zhong, Z.: Graphene photodetectors with ultra-broadband and high responsivity at room temperature. *Nat. Nanotechnol.* **9**(4), 273–278 (2014)
- Ludbrook, B.M., et al.: Evidence for superconductivity in Li-decorated monolayer graphene. *Proc. Nat. Acad. Sci.* **112**(38), 11795–11799 (2015)
- Margine, E.R., Giustino, F.: Two-gap superconductivity in heavily  $n$ -doped graphene: Ab initio migdal-eliasberg theory. *Phys. Rev. B* **90**, 014518 (2014)
- Margine, E., Lambert, H., Giustino, F.: Electron-phonon interaction and pairing mechanism in superconducting ca-intercalated bilayer graphene. *Sci. Rep.* **6**, 21414 (2016)
- Masir, M.R., Moldovan, D., Peeters, F.: Pseudo magnetic field in strained graphene: revisited. *Solid State Commun.* **175**, 76–82 (2013)
- Matković, A., Milošević, I., Miličević, M., Tomašević-Ilić, T., Pešić, J., Musić, M., Spasenović, M., Jovanović, D., Vasić, B., Deeks, C., Panajotović, R., Belić, M.R., Gajić, R.: Enhanced sheet conductivity of Langmuir-Blodgett assembled graphene thin films by chemical doping. *2D Mater.* **3**(1), 015002 (2016)
- Mazin, I., Balatsky, A.: Superconductivity in Ca-intercalated bilayer graphene. *Philos. Mag. Lett.* **90**(10), 731–738 (2010)
- Nakada, K., Ishii, A.: DFT calculation for adatom adsorption on graphene. In: Gong, J.R. (ed.) *Graphene Simulation*. InTech, Rijeka, Croatia (2011)
- Neto, A.H.C., Guinea, F., Peres, N.M.R.: Edge and surface states in the quantum hall effect in graphene. *Phys. Rev. B* **73**, 205408 (2006)
- Novoselov, K.S., Geim, A.K., Morozov, S.V., Jiang, D., Zhang, Y., Dubonos, S.V., Grigorieva, I.V., Firsov, A.A.: Electric field effect in atomically thin carbon films. *Science* **306**(5696), 666–669 (2004)
- Novoselov, K.S., Jiang, Z., Zhang, Y., Morozov, S.V., Stormer, H.L., Zeitzer, U., Maan, J.C., Boebinger, G.S., Kim, P., Geim, A.K.: Room-temperature quantum hall effect in graphene. *Science* **315**(5817), 1379–1379 (2007)
- Penev, E.S., Kutana, A., Yakobson, B.I.: Can two-dimensional boron superconduct? *Nano Lett.* **16**(4), 2522–2526 (2016)
- Perdew, J.P., Zunger, A.: Self-interaction correction to density-functional approximations for many-electron systems. *Phys. Rev. B* **23**, 5048–5079 (1981)
- Peres, N.M.R., Neto, A.H.C., Guinea, F.: Conductance quantization in mesoscopic graphene. *Phys. Rev. B* **73**, 195411 (2006)
- Pešić, J., Gajić, R., Hingerl, K., Belić, M.: Strain-enhanced superconductivity in Li-doped graphene. *EPL (Europhys. Lett.)* **108**(6), 67005 (2014)
- Pešić, J., Damjanović, V., Gajić, R., Hingerl, K., Belić, M.: Density functional theory study of phonons in graphene doped with Li, Ca and Ba. *EPL (Europhys. Lett.)* **112**(6), 67006 (2015)
- Profeta, G., Calandra, M., Mauri, F.: Phonon-mediated superconductivity in graphene by lithium deposition. *Nat. Phys.* **8**(2), 131–134 (2012)
- Qu, L., Liu, Y., Baek, J.B., Dai, L.: Nitrogen-doped graphene as efficient metal-free electrocatalyst for oxygen reduction in fuel cells. *ACS Nano* **4**(3), 1321–1326 (2010)
- Rüdorff, W.: Graphite Intercalation Compounds. *Advances in Inorganic Chemistry and Radiochemistry*, pp. 223–266. Academic Press, Cambridge (1959)
- Saito, Y., Nojima, T., Iwasa, Y.: Highly crystalline 2d superconductors. *Nat. Rev. Mater.* **2**, 16094 (2016)
- Sassi, U., Parret, R., Nanot, S., Bruna, M., Borini, S., De Fazio, D., Zhao, Z., Lidorikis, E., Koppens, F., Ferrari, A., et al.: Graphene-based mid-infrared room-temperature pyroelectric bolometers with ultra-high temperature coefficient of resistance. *Nature Commun.* **8**, 14311 (2017)
- Settnes, M., Power, S.R., Jauho, A.P.: Pseudomagnetic fields and triaxial strain in graphene. *Phys. Rev. B* **93**, 035456 (2016)
- Sharma, B.K., Ahn, J.H.: Graphene based field effect transistors: efforts made towards flexible electronics. *Solid-State Electron.* **89**(Supplement C), 177–188 (2013)
- Shimada, N.H., Minamitani, E., Watanabe, S.: Theoretical prediction of phonon-mediated superconductivity with  $T_c = 25K$  in Li-intercalated hexagonal boron nitride bilayer. *Appl. Phys. Express* **10**(9), 093101 (2017)
- Si, C., Liu, Z., Duan, W., Liu, F.: First-principles calculations on the effect of doping and biaxial tensile strain on electron-phonon coupling in graphene. *Phys. Rev. Lett.* **111**, 196802 (2013)

- Todorović, D., Matković, A., Milićević, M., Jovanović, D., Gajić, R., Salom, I., Spasenović, M.: Multilayer graphene condenser microphone. *2D Mater* **2**(4), 045013 (2015)
- Wakabayashi, K., Fujita, M., Kusakabe, K., Nakada, K.: Magnetic structure of graphite ribbon. *Czech J. Phys.* **46**(4), 1865–1866 (1996)
- Wakabayashi, K., Takane, Y., Yamamoto, M., Sigrist, M.: Edge effect on electronic transport properties of graphene nanoribbons and presence of perfectly conducting channel. *Carbon* **47**(1), 124–137 (2009)
- Wang, Y., Shao, Y., Matson, D.W., Li, J., Lin, Y.: Nitrogen-doped graphene and its application in electrochemical biosensing. *ACS Nano* **4**(4), 1790–1798 (2010)
- Weller, T.E., Ellerby, M., Saxena, S.S., Smith, R.P., Skipper, N.T.: Superconductivity in the intercalated graphite compounds  $C_6Yb$  and  $C_6Ca$ . *Nat. Phys.* **1**(1), 39–41 (2005)
- Xue, M., Chen, G., Yang, H., Zhu, Y., Wang, D., He, J., Cao, T.: Superconductivity in potassium-doped few-layer graphene. *J. Am. Chem. Soc.* **134**(15), 6536–6539 (2012)